SARI METSÄMÄKI

A fractional snow cover mapping method for optical remote sensing data, applicable to continental scale

Aalto University, School of Engineering,

Department of Real Estate, Planning and Geoinformatics

2013

A fractional snow cover mapping method for optical remote sensing data, applicable to continental scale

Sari Metsämäki

Aalto University School of Engineering
Department of Real Estate, Planning and Geoinformatics
Doctoral dissertation in Remote Sensing

Dissertation for the degree of Doctor of Science in Technology to be presented for public examination with the permission of the Aalto University School of Engineering (Espoo, Finland), in Auditorium E (Y124), Otakaari 1, Espoo, on August 23, 2013, at 12 o'clock noon.

Espoo 2013

Supervising professor:	Professor Henrik Haggren, Aalto University, School of Engineering, Department of Real Estate, Planning and Geoinformatics, Espoo
Preliminary examiners:	Dr., Professor Richard Kelly University of Waterloo, Department of Geography and Environmental Management, Ontario, Canada
	Dr., Professor David A. Robinson Rutgers University, Department of Geography & Office of the State Climatologist, New Jersey, USA
Opponents:	Dr., Research Professor Tuomas Häme VTT Technical Research Centre of Finland, Espoo
	Dr., Professor Richard Kelly University of Waterloo, Department of Geography and Environmental Management, Ontario, Canada

ISBN 978-952-93-2556-6 (paperback)
ISBN 978-952-93-2557-3 (PDF)
http://urn.fi/URN:ISBN:978-952-93-2557-3

Edita Prima Ltd
Helsinki 2013

Contents

List of appended papers and author´s contribution

This thesis is based on the work published in the following scientific papers (peer-reviewed journal publications):

[P1] Metsämäki S., Vepsäläinen J., Pulliainen J. & Sucksdorff Y. (2002). Improved linear interpolation method for the estimation of snow-covered area from optical data, *Remote Sensing of Environment, 82, 64-78.*

[P2] Metsämäki, S., Anttila, S., Huttunen, M. & Vepsäläinen, J. (2005). A feasible method for fractional snow cover mapping in boreal zone based on a reflectance model. *Remote Sensing of Environment*, *95, 77-95.*

[P3] Salminen, M., Pulliainen, J., Metsämäki, S., Kontu, A. & Suokanerva, H. (2009).
The behaviour of snow and snow-free surface reflectance in boreal forests: Implications to the performance of snow covered area monitoring. *Remote Sensing of Environment, 113, 907-918.*

[P4] Metsämäki, S., Mattila, O.-P., Pulliainen, J., Niemi, K., Luojus, K. & Böttcher, K. (2012). An optical reflectance model-based method for fractional snow cover mapping applicable to continental scale. *Remote Sensing of Environment, 123, 508-521.*

[P5] Niemi, K., Metsämäki, S., Pulliainen, J., Suokanerva, H., Böttcher, K., Leppäranta, M. & Pellikka, P. (2012). The behaviour of mast-borne spectra in a snow-covered boreal forest. *Remote Sensing of Environment, 124, 551-563.*

In publication **[P1]**, S. Metsämäki was (together with J. Vepsäläinen) responsible for method development, implementation to AVHRR-data and for the validations. Particularly, S. Metsämäki was responsible for the work related to wet snow detection from AVHRR times-series and NDVI-rule for snow-free ground detection.

In publication **[P2]**, S. Metsämäki (together with J. Vepsäläinen and S. Anttila) carried out the method development, implementation and validation. In addition, S. Metsämäki was particularly responsible for the statistical accuracy assessment and the transmissivity-related NDVI-thresholding for snow-free ground detection.

For publication **[P3]**, S. Metsämäki largely contributed to designing of the field spectroscopy measurements, data analyses and the driven conclusions. Her particular contribution was related to statistical accuracy.

In publication **[P4]**, S. Metsämäki was the principal author, solely responsible for the topic, structure and contents of the paper, data processing, implementations and analyses as well as for validations. Contributions from the other authors were mainly supportive.

For publication **[P5]**, S. Metsämäki largely contributed in data analyses and in the driven conclusions, particularly concerning the evaluation of the feasibility of NDSI in fractional snow mapping as well as the simulations of the scene spectra.

List of acronyms and symbols

Acronyms

AATSR	Advanced Along-Track Scanning Radiometer
ASD	Analytical Spectral Devices
AVHRR	Advanced Very High Resolution Radiometer
BHR	Spectral Bi-hemispherical Reflectance
BRF	Bidirectional Reflectance Factor
BRDF	Bidirectional Reflectance Distribution Function
DHR	Directional-Hemispherical Reflectance
EOS	Earth Observing System
ETM+	Enhanced Thematic Mapper +
FMI	Finnish Meteorological Institute
FSC	Fractional Snow Cover
HDRF	Hemispherical-directional Reflectance Factor
MODIS	Moderate Resolution Imaging Spectroradiometer
NASA	National Aeronautics and Space Administration
NDSI	Normalized Difference Snow Index
NDVI	Normalized Difference Vegetation Index
NIR	Near-infrared
NOAA	National Oceanic and Atmospheric Administration
NSIDC	National Snow and Ice Data Center
RMSE	Root Mean Squared Error
SCA	Snow-covered area
SCAmod	Fractional snow cover retrieval method
SD	Snow Depth
SMAC	Simplified Method for Atmospheric Corrections
SYKE	Finnish Environment Institute
SWE	Snow Water Equivalent
SWIR	Shortwave infrared
TM	Thematic Mapper
TOA	Top-of-atmosphere
VGF	Viewable Gap Fraction
VIS	Visible
WMO	World Meteorological Organization

Symbols

α	albedo [dimensionless]
θ_0	zenith angle of the incoming radiance [rad]
θ_S	zenith angle of the reflected radiance [rad]
λ	wavelength [m]
$\rho_{\lambda,snow}$	snow reflectance at wavelength λ [dimensionless]
$\rho_{\lambda,drysnow}$	dry snow reflectance at wavelength λ [dimensionless]
$\rho_{\lambda,ground}$	snow-free ground reflectance at wavelength λ [dimensionless]
$\rho_{\lambda,forest}$	opaque forest canopy reflectance at wavelength λ [dimensionless]
$\rho_{\lambda,obs}$	observed scene reflectance at wavelength λ [dimensionless]
φ_0	azimuth angle of the incoming radiance [rad]
φ_S	azimuth angle of the reflected radiance [rad]
Ω	solid angle [rad]
$E_0(\theta_0, \varphi_0, \lambda)$	incident solar irradiance at wavelength λ in direction θ_0, φ_0 [$Wm^{-2}sr^{-1}$]
F_{snow}	areal fraction of snow-covered ground within the pixel [dimensionless]
F_{ground}	areal fraction of snow-free ground [dimensionless]
$L(\theta, \varphi, \lambda)$	reflected radiance at wavelength λ in the direction θ, φ [$Wm^{-2}sr^{-1}$]
R1	reflectance at Band 1 (visible) of AVHRR [dimensionless]
R2	reflectance at Band 2 (near-infrared) of AVHRR [dimensionless]
S^2_{snow}	variance of reflectance of snow [dimensionless]
S^2_{forest}	variance of reflectance of forest canopy [dimensionless]
S^2_{ground}	variance of reflectance of snow-free ground [dimensionless]
t^2_λ	two-way transmissivity at wavelength λ [dimensionless]

A fractional snow cover mapping method for optical remote sensing data, applicable to continental scale

Sari Metsämäki

Aalto University, School of Engineering, Department of Real Estate, Planning and Geoinformatics

Metsämäki, S. 2013. A fractional snow cover mapping method for optical remote sensing data, applicable to continental scale. Monographs of the Boreal Environment Research No. 43. 53 p.

Abstract

This thesis focuses on the determination of fractional snow cover (FSC) from optical data provided by satellite instruments. It describes the method development, starting from a simple regionally applicable linear interpolation method and ending at a globally applicable, semi-empirical modeling approach. The development work was motivated by the need for an easily implementable and feasible snow mapping method that could provide reliable information particularly for forested areas.

The contribution of the work to the optical remote sensing of snow is mainly associated with accounting for boreal forest canopy effect to the observed reflectance, thus facilitating accurate fractional snow retrievals also for ground beneath the tree canopies. The first proposed approach was based on a linear interpolation technique, which relies on *a priori known reference reflectances* at a) full snow cover and b) snow-free conditions for each calculation unit-area. An important novelty in the methodology was the utilization of a *forest sparseness index* determined from AVHRR reflectance data acquired at full dry snow cover conditions. This index was employed to describe the similarity between different unit-areas. In practice, the index was used to determine the reference reflectances for such unit-areas for which the reflectance level could not be determined otherwise, e.g. due to frequent cloud cover. This approach was found to be feasible for Finnish drainage basins characterized by fragmented landscape with moderate canopies.

Using a more physical approach instead of linear interpolation would allow the model parameterization using physical quantities (reflectances), and would therefore leave space for further model developments based on measuring and/or modeling of these quantities. The semi-empirical reflectance model-based method *SCAmod* originates from radiative transfer theory and describes the scene-level reflectance as a mixture of three major constituents: opaque forest canopy, snow and snow-free ground, which are interconnected through transmissivity and snow fraction. Transmissivity, in turn, can be derived from reflectance observations under conditions that highlight the presence of forest canopy, namely the presence of full snow cover on the ground. Thus, SCAmod requires *a priori* information on transmissivity, but given that it can be determined with the appropriate accuracy, it enables consideration of the obstructing effects of forests in fractional snow estimation. In continental-scale snow mapping, determination of the transmissivity map becomes a key issue. The preliminary demonstration of transmissivity generation using global land cover data was a part of this study.

The first implementations and validations for SCAmod were presented for AVHRR data at Finnish drainage basin scale. In subsequent work, determination of the feasible reflectance constituents was addressed, followed by a sensitivity analysis targeting at selection of optimal spectral bands to be applied with SCAmod. Feasibility of the NDSI-based approach in FSC-retrievals over boreal forests is also discussed. Finally, the implementations and validations for MODIS and AATSR data are presented. The results from relative (using high-resolution Earth Observation data to represent the truth) and absolute validation (using *in situ* observations)

indicate a good performance for both forested and non-forested regions in northern Eurasia. Accounting for the effect of forest canopy in the FSC-retrievals is the key issue in snow remote sensing over boreal regions; this study provides a new contribution to this research field and provides one solution for continental scale snow mapping.

Keywords: Snow, Fractional snow cover, Boreal zone, Forests, Tundra, Optical remote sensing

Menetelmä lumen peittämän alan mannertenlaajuiseen kartoitukseen optisilta satelliittikuvilta

Sari Metsämäki

Aalto-yliopisto, Insinööritieteiden korkeakoulu, Maankäyttötieteiden laitos

Metsämäki, S. 2013. A fractional snow cover mapping method for optical remote sensing data, applicable to continental scale. Monographs of the Boreal Environment Research No. 43. 53 p.

Tiivistelmä

Tämä väitöskirja käsittelee optisen alueen satelliittikaukokartoitusaineistojen käyttöä lumipeitteen kartoitukseen. Tavoitteena on saada luotettavaa tietoa lumen peittävyydestä (FSC, Fractional Snow Cover) erityisesti boreaalisen metsävyöhykkeen ja tundravyöhykkeen alueilla. Väitöskirjassa kuvataan menetelmäkehityksen vaiheet lähtien lineaarisesta interpolaatiosta ja päätyen globaalisti sovellettavaan semiempiiristä heijastusmallia hyödyntävään menetelmään. Luotettavan tiedon saaminen lumen peittävyydestä varsinkin metsäisillä alueilla on haastavaa monille kaukokartoitusmenetelmille. Työn keskeisenä tuloksena on menetelmä, jolla saadaan tietoa lumipeitteestä jopa tiheiden metsien tapauksessa.

Ensimmäiseksi kehitetyllä lineaariseen interpolaatioon perustuvalla menetelmällä tuotettiin valuma-aluetason tietoa lumipeitteen laajuudesta Suomen ympäristökeskuksen tulvaennusteiden käyttöön. Siinä jokaiselle laskentayksikölle määritettiin sille tyypillinen heijastusarvo 100 % lumipeitteen (märkä eli sulava lumi) että vastaavasti lumettoman tilanteen aikana; sulamisaikaan lumen peittävyys estimoitiin interpoloimalla näiden kahden ääriarvon välillä. Työssä kehitettiin menetelmä ääriarvojen määrittämiseen NOAA/AVHRR-instrumentin tuottamilta kuvilta. Erityistä huomiota kiinnitettiin ääriarvojen määrittämiseen tarvittavan kaukokartoitushavainnon puuttuessa esimerkiksi pilvisyyden vuoksi. Tähän löydettiin ratkaisuksi ottaa ääriarvo läheiseltä, mahdollisimman samankaltaiselta alueelta. Koska varsinkin lumisessa tilanteessa boreaalisen metsän vaikutus havaittuun heijastukseen on suuri, on laskentayksikön metsäisyys merkittävin kriteeri samankaltaisuutta arvioitaessa. Metsäisyyttä kuvaamaan kehitettiin ns. harvuusindeksi, joka laskettiin jokaiselle laskentayksikölle käyttäen eri vuosina havaittuja lumisen ajankohdan heijastusarvoja. Menetelmän todettiin toimivan hyvin Suomen valuma-alueille, joihin lähes kaikkiin lukeutuu sekä metsäisiä että avoimia alueita.

Fysikaalinen heijastusmallinnus on lineaarista interpolaatiota edistyneempi lähestymistapa lumipeitteen kaukokartoitukseen, sillä mallin tekijät kuvaavat mitattavissa olevia suureita. Optisen kaukokartoituksen tapauksessa mitattavat suureet ovat eri luonnonkohteiden heijastusarvoja (reflektansseja). Työssä kehitetty SCAmod-menetelmä käyttää semiempiiristä säteilynkuljetusteoriaan perustuvaa heijastusmallia lumen peittävyyden estimointiin. Malli

kuvaa kohteesta mitattavan heijastuksen lumen, lumettoman maan sekä metsän heijastusten kombinaationa. Näiden kolmen eri tekijän vaikutus havaittuun heijastukseen riippuu ensinnä lumisen ja lumettoman maan suhteesta sekä toiseksi metsän peittävyydestä, tarkemmin sanoen sen transmissiivisyydestä. Jos lumen, lumettoman maan ja metsän heijastukset sekä laskentayksikön transmissiivisyys tunnetaan, voidaan havaitusta heijastuksesta laskea lumen peittävyys. Koska näiden kolmen heijastustekijän heijastusarvot ovat mitattavia suureita, päästään käsiksi myös heijastusarvojen vaihteluun sekä tämän vaihtelun aiheuttamaan epätarkkuuteen lumen peittävyyden estimoinnissa. Transmissiivisyys puolestaan on laskettavissa SCAmodin heijastusmallista käyttäen täyden lumipeitteen aikana tehtyjä heijastushavaintoja. Globaalissa mittakaavassa transmissiivisyyden määrittäminen suoraan heijastushavainnoista on käytännössä mahdotonta koska pilvettömiä, täyden lumipeitteen havaintoja ei varmuudella ole saatavissa. Tässä työssä esitetäänkin menetelmä pohjoisen pallonpuoliskon transmissiivisyyskartan määrittämiseksi käyttäen maankäyttö/kasvillisuuskarttaa.

SCAmod-menetelmä toteutettiin ensin AVHRR-kuville ja Suomen valuma-alueille. Samalla tutkittiin kuinka lumen peittävyysestimaattien tilastollista tarkkuutta voidaan arvioida. Seuraavaksi paneuduttiin heijastustekijöiden tarkempaan määrittämiseen sekä selvitettiin eri aallonpituuskanavien sopivuus menetelmän käyttöön. Työssä on myös käsitelty NDSI:n (Normalized Difference Snow Index) soveltuvuutta lumen peittävyyden määrittämiseen boreaalisessa metsässä. SCAmod-menetelmän soveltuvuutta pohjoisen pallonpuoliskon kausittaisen lumipeitteen kartoittamiseen tutkittiin keskiresoluution MODIS- ja AATSR-kuvia käyttäen. Lumen peittävyysestimaatteja validoitiin käyttäen korkean resoluution satelliittikuvia sekä Suomessa tehtyjä maastohavaintoja. Työssä todetaan menetelmän soveltuvan hyvin boreaalivyöhykkeen ja tundravyöhykkeen lumikartoitukseen; erityisesti SCAmodilla saadaan tietoa myös metsäisiltä alueilta, mikä tekee siitä varteenotettavan menetelmän korvaamaan tai täydentämään muita yleisesti käytössä olevia lumikaukokartoitusmenetelmiä.

Asiasanat: Lumi, Lumipeite, Boreaalinen vyöhyke, Metsät, Tundra, Optinen kaukokartoitus

1 Introduction

1.1 Background

Snow cover has an important role in Earth Sciences. Through its high albedo, snow strongly affects the Earth's radiation budget in both global and regional scales. As a massive reserve of stored water, snow is an essential part of the hydrological cycle. Reliable information concerning seasonal, inter-annual and long-term changes in snow extent and characteristics is important for climate change studies and water management (e.g. Gong et al., 2007; Kitaev et al., 2002; Kite and Pietroniro, 1996; Choi et al., 2010; Robinson and Frei, 2000; Roesch and Roeckner, 2006; Schmugge et al., 2002; Viterbo and Betts, 1999). Since seasonal snow accumulation and melting usually concern extensive areas with varying climatic features, resulting in highly different timings of these processes, it has been essential to aim at development of such methods that provide spatially and temporally frequent information on snow cover. Remote sensing provides a feasible way to accomplish this. Both the extent of the snow cover and the characteristics of the snow pack can be investigated. With current remote sensing techniques, the typically targeted characteristics are Snow water equivalent, Snow depth, Snow liquid water content, Snow surface temperature, Snow grain size and Snow albedo. These can be derived using data provided by sensors operating in the optical or microwave region with a variety of methods.

The extent of snow cover is typically expressed as two-class information, i.e. assigning each pixel as snow-covered or as snow-free. This is called *binary* snow data and is a relatively good measure of snow extent in many applications. However, discriminating between these two cases is rather vague, because in nature, seasonal snow depletion appears as patchy snow before the final clearance, see Fig. 1-1. Depending on the application and scale, we usually need to know whether a pixel is fully snow covered or if it has a lower snow fraction or is absolutely snow-free. A step forward from binary information is Fractional Snow Cover (FSC), also known as fraction of Snow Covered Area (SCA), which features the areal fraction of snow cover within a pixel. FSC gives a percentage number for snow coverage, which is considered more informative than binary data. Several methods for retrieving FSC from remote sensing data have been developed; typically, they suffer from inaccuracies over forest areas. The presence of forest canopy poses a problem for snow-retrievals, since the canopy obscures the sensor's view to the snow (or snow-free ground) beneath it. Several methodologies have been developed to better adjust to the presence of forest but with varying success (Hall et al., 2007; Klein et al., 1998; Rittger et al., 2012; Salomonson and Appel, 2004; Vikhamar and Solberg, 2003). Considering that forests constitute a rather high proportion of seasonally snow-covered regions in the northern hemisphere, this is a serious defect.

This thesis focuses on the determination of FSC from optical data provided by satellite instruments, and describes the method development starting from a simple regionally applicable linear interpolation method and ending in a globally applicable semi-empirical modeling approach. The development work was motivated by the need for an easily implementable and feasible snow monitoring method that could also provide reliable information for forested areas.

This work mainly deals with fractional snow cover estimation in boreal forests and tundra areas using a semi-empirical radiative transfer-based reflectance model, which expresses the observed reflectance as a function of FSC. The essence of the model is the *apparent forest transmissivity*, related to the visibility of the under-canopy ground when observed above the canopy. Modeling (or otherwise correcting) the effect of forest canopy in FSC-retrievals is the key issue in snow remote sensing over boreal regions; this study contributes to the advancements in this research field and provides a new contribution to continental scale snow mapping.

Figure 1-1. Fractional snow cover in a boreal forest in northern Finland, from **[P4]**.

1.2 Basics of optical remote sensing of fractional snow cover

An important factor in the Earth's radiation balance is the surface albedo α, describing the ratio of reflected radiation $\mathrm{I}\uparrow$ to incoming solar irradiation $\mathrm{I}\downarrow$

$$\alpha = \mathrm{I}\uparrow / \mathrm{I}\downarrow = \frac{\int_{2\pi} L(\theta,\varphi,\lambda)\partial\Omega}{\int_{2\pi} E_0(\theta_0,\varphi_0,\lambda)\partial\Omega} \tag{1-1}$$

where $L(\theta,\varphi,\lambda)$ [$\mathrm{Wm^{-2}sr^{-1}}$] is the reflected radiance at wavelength λ and $E_0(\theta_0,\varphi_0,\lambda)$ [$\mathrm{Wm^{-2}sr^{-1}}$] is the incident solar irradiance. The albedo depends on the directional distribution of incoming radiation, except for Lambertian surfaces, which reflect evenly in all directions. The direction-dependence can be expressed as a *bidirectional reflectance distribution function (BRDF)*

$$BRDF(\theta_0,\theta,\varphi_0,\varphi,\lambda) = \frac{L(\theta,\varphi,\lambda)}{\cos(\theta_0)E_0(\theta_0,\varphi_0,\lambda)} \tag{1-2}$$

Hence, given a certain illumination direction and power, BRDF determines the radiation power in a viewing direction, which is what the satellite instrument observes. When this is normalized with respect to the BRDF from an ideal, lossless and diffuse (Lambertian) surface under the same illumination and viewing directions, we obtain the *bidirectional reflectance factor BRF*. This is the

quantity often used when referring to *reflectance* in the field of satellite remote sensing (Schaepmann-Strub et al., 2006):

$$BRF(\theta_0,\theta,\varphi_0,\varphi,\lambda) = \frac{BRDF(\theta_0,\theta,\varphi_0,\varphi,\lambda)}{BRDF_{ideal}(\theta_0,\theta,\varphi_0,\varphi,\lambda)} = \frac{BRDF(\theta_0,\theta,\varphi_0,\varphi,\lambda)}{1/\pi} = \pi \cdot BRDF(\theta_0,\theta,\varphi_0,\varphi,\lambda) \quad (1\text{-}3)$$

The reflectance factor may exceed 1, particularly for strongly forward scattering surfaces such as snow (Jin and Simpson, 1999; Painter and Dozier, 2004; Peltoniemi et al., 2005).

The *spectral bi-hemispherical reflectance BHR* is then an integral of BRDF over all illumination and reflection angles, and is generally referred to as albedo. Under conditions of pure diffuse isotropic illumination, the resulting BHR is generally called *white-sky albedo*. If the illumination comes from a single direction only, the resulting quantity is *directional-hemispherical reflectance DHR*, generally called *black-sky albedo*.

Snow has a very high albedo compared to other natural land covers. The albedo is highest at visible wavelengths and decreases towards infrared. In all wavelengths, the albedo decreases with increasing grain size and increases at lower solar elevations (Wiscombe and Warren, 1980; Warren, 1982). Snow is typically a strongly anisotropic reflector, exhibiting a peak in forward scattering directions. Several studies related to the modeling and measurement of anisotropy have been carried out, often related to grain size variations (Dozier, 1981; Jin and Simpson, 1999; Nolin and Dozier, 2000; Painter and Dozier, 2004; Painter et al., 2009; Peltoniemi et al., 2005; Steffen, 1987; Warren, 1982; Wiscombe and Warren, 1980). From these it has been concluded that the reflectance anisotropy is stronger at near-infrared wavelength than in visible wavelengths, and that larger grain size still induces higher anisotropy.

The optical remote sensing of snow strongly relies on the fact that at visible wavelengths, snow has very high BRF (hereafter referred to as *reflectance*), whereas the reflectance decreases distinctively towards shortwave-infrared. For vegetation and soil, the trend is the opposite. The visible reflectance from snow alters according to snow properties such as grain size and impurity, but still remains high compared to shortwave-infrared reflectance (Dozier et al., 1981, 1989; Nolin and Dozier, 2000; Painter and Dozier, 2004; Warren, 1982). The spectral characteristics of snow are utilized in the calculation of Normalized Difference Snow index (NDSI), which is defined as a ratio of visible (VIS) and shortwave-infrared (SWIR) reflectance as follows (Riggs et al., 1994; Hall et al., 1995):

$$NDSI = (VIS - SWIR)/(VIS + SWIR) \quad (1\text{-}4)$$

Hence, the high reflectance of snow in the visible compared with the short-wave infrared part of the spectrum yields high NDSI values for snow compared with other natural targets.

The typical reflectance spectra from dry and wet snow, as measured with an ASD-spectrometer at the test site in Sodankylä, Finland, are presented in Fig. 1-2.

In the presence of forest canopy partly obstructing the view to the ground, the problem for snow detection is related to the fact that the observed reflectance is a mixture of reflectances from snow, snow-free ground and forest canopy. The effect of forest canopy depends on canopy characteristics such as crown coverage, biomass and canopy structure in general, but also on the illumination and viewing geometries (e.g. Betts and Ball, 1997; Hall et al., 1998; Liu et al., 2008; Robinson and Kukla, 1985; Xin et al., 2012). Understanding and modeling of these effects pose a challenge for fractional snow cover retrievals.

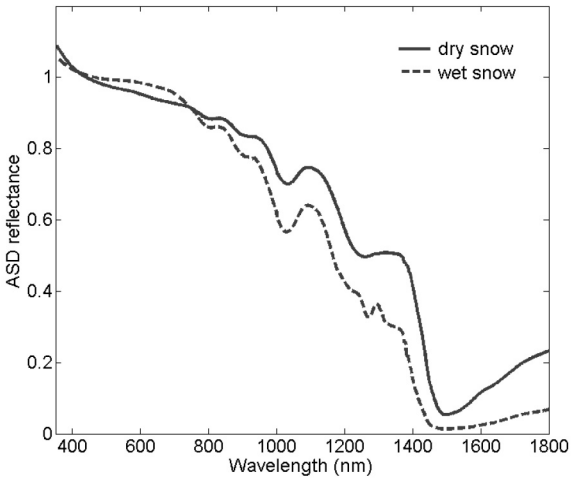

Figure 1-2. Reflectance spectra from dry and wet snow, as measured with an ASD-spectrometer.

1.3 Advances in optical remote sensing of (fractional) snow cover

Several approaches have been developed for deriving the fraction of snow covered area from optical remote sensing data. The *spectral unmixing methods* typically utilize several spectral bands and a variety of spectral end-members and least-square techniques to solve the FSC from the spectral mixture model (e.g. Painter et al., 2003). Linear spectral mixture analysis considers the observed reflectance as a linear combination of reflectances from certain surface constituents (end-members) (e.g. Solberg et al., 2003). Accordingly, the use of only two end-members – snow-covered ground and snow-free ground - reduces FSC derivation to a linear interpolation problem (Matikainen et al., 2002; Metsämäki et al., 2002). This approach has also been used with microwave radar data (Koskinen et al., 1997). Considering the different land covers in different parts of seasonally snow-covered regions, the end-members should be adapted to locality in order to obtain accurate estimates of FSC. This concerns particularly the different types of forests (broadleaf, needle leaf) and their densities as well as different types of snow-free ground, e.g. rock, grassland, shrubland and different soils. The spectral unmixing methods often employ soil/snow/canopy models to determine the spectral end-members. For example, introducing the method *SnowFrac*, Vikhamar et al. (2004) described how topography and forest canopy effects can be modeled and used as input to the spectral unmixing method. The *MODSCAG* method of Painter et al. (2009) used a radiative transfer model specific for the scene illumination and view geometry to retrieve the snow spectral end-members with varying grain size. Liu et al. (2008) and Xin et al. (2012) modeled the Viewable Gap Fraction (VGF) for different forest types and with different view and illumination geometries and emphasized the importance of these geometries in FSC-retrievals.

The *methods utilizing NDSI* rely on the ratio of observed reflectances at visible and short-wave-infrared bands, so that high NDSI is provided by snow-covered surfaces. The snow mapping method proposed by Hall et al. (1995) designates a pixel as snow-covered if NDSI>0.4. Klein et al. (1998) proposed an improved method to better account for forests. The modified method uses snow and canopy reflectance models to expand the acceptance area for NDSI; this is accomplished by employment of NDVI in addition to NDSI. Tests for visible reflectance were also added. This approach gives binary information on snow cover, i.e. it tells whether a pixel is snow-covered or not. It is still one of the baseline methods for MODIS snow mapping products distributed by the National Snow and Ice Data Center (Hall et al., 2006a, 2006b). To derive information on the fraction of snow cover on a pixel level, Salomonson and Appel (2004) proposed a method in

which FSC is related to the magnitude of NDSI. This was accomplished through ordinary linear regression, using FSC from high-resolution Landsat TM-imagery as 'truth'.

Since variation of grain size is one of most prominent characteristics related to snow, the effects of grain size on albedo and bidirectional reflectance factor (BRF) have been widely studied. Measurements of BRF have been conducted in several field campaigns (Dumont et al., 2010; Painter and Dozier, 2004; Peltoniemi et al., 2005; Steffen, 1987). These are important contributions in the way towards more accurate FSC-retrievals from remote sensing data.

Overall, the handicap with many of the methodologies has been and still is their poorer performance in forested areas (e.g. Frei et al., 2012). This poses a need for better considerations of the effect of forest in the remote sensing observations.

Contribution of the appended papers

The contribution of the present work to the optical remote sensing of snow is mostly related to the modeling and accounting for boreal forest canopy effect on the observed reflectance, targeting at accurate fractional snow retrievals also for ground beneath the tree canopies. The first proposed approach in **[P1]** was based on a linear interpolation technique, which relies on *a priori known reference reflectances* at a) full snow cover and b) snow-free conditions for each calculation unit-area. An important novelty in the methodology was the utilization of a *forest sparseness index* determined from clear-sky AVHRR reflectance data acquired at full snow cover conditions. This index was employed to describe the similarity between different unit-areas. In practice, the index was used to determine the reference reflectances for unit-areas for which the reflectance level could not be determined otherwise, e.g. due to frequent cloud cover. This approach was found to be feasible for Finnish drainage basins, characterized by fragmented landscape with moderate canopies. Employing reflectance observations from full snow-covered forests to map forest properties was earlier proposed e.g. by Nolin (2004) and Hall et al. (1998). However, the idea of using the observed reflectance to derive *apparent forest transmissivity* for FSC retrievals was a novelty, introduced in **[P2]**. Through transmissivity, the proposed radiative transfer-based reflectance model relates the observed reflectance to the major reflective constituents: forest canopy, snow and snow-free ground. FSC is included in the model to describe the areal proportions of the latter two. Hence, FSC can be solved from observed reflectance, given that the transmissivity and the representative values for the three reflective constituents are known. The method was named *SCAmod*; the first implementations and validations were presented for AVHRR data at the Finnish drainage basin scale. The principles for statistical accuracy assessment for SCAmod FSC retrievals were also presented in **[P2]**. In further studies (**[P3]** and **[P5]**), determination of the feasible reflectance constituents was addressed, followed by a sensitivity analyses, targeting at selection of optimal spectral bands to be applied with SCAmod. **[P5]** also discussed the feasibility of the NDSI-based approach in FSC-retrievals over dense boreal forests. Finally, **[P4]** presented the implementations and validations for MODIS and AATSR data. A new approach to enable the continental-scale use of SCAmod was introduced, related to the hemispherical transmissivity generation with a tolerable effort. The results from relative and absolute validation indicate a good performance for both forested and non-forested regions in Northern Eurasia.

2 Materials and methods

2.1 Study area

The studies in this thesis focus on the boreal forest and sub-arctic zone in northern and eastern Europe. These areas are characterized by seasonal snow and feature boreal and hemi-boreal landscapes as well as tundra and steppe/agricultural areas. The specific interest lies in Finland (~338,000 km²), located in 60-70°N, 20-30°E, between Sweden and Russia. Finland provides an extensive dataset of *in situ* snow measurements, which enable method development and validations in a unique manner. Finland is significantly covered by boreal forests, open bogs, lakes and agricultural area, but in the north, tundra regions are also widespread. Typically the forests are relatively sparse (METLA, 2009). Dominant tree species are Scots pine and Norway spruce, but small birches are also common especially in high-altitude fell-regions. No significant altitude variations occur on average. The seasonal snow cover typically settles in November-December and persists until April-June; the average annual snow water equivalent reaches 140-200 mm in the north and 80-140 mm in the south. In southern Finland the snow cover usually persists for four months, and includes repeated freezing and thawing processes, whereas further north the snow layer is more homogenous and tends to persist for more than 6 months (Kuusisto, 1984).

Finland belongs to the Baltic Sea drainage area, except that some northernmost basins drain to the Arctic Ocean or the White Sea. The method development first targeted the provision of high-accuracy fractional snow information for Finnish and cross-boundary watersheds for the needs of hydrological modeling (**[P1] and [P2]**). Encouraged by the success of the SCAmod approach for Finland, the target area was gradually expanded to regional and continental scales. Although Finland represents a wide variety of boreal landscapes, the inclusion of other regions in northern and eastern Europe would complement the study area since they feature all the relevant land covers and landscapes as well as different snow types in continental scale (excluding mountains). The very dense forests in Russia are of particular interest. Consequently, in **[P4],** the areas from the Ural mountains in the east to Sweden in the west, and from the Barents Sea in the north to Ukraine in the south were studied. The study area is presented in Fig. 2-1, also featuring the high-resolution data scenes used in the validations (**[P4]**).

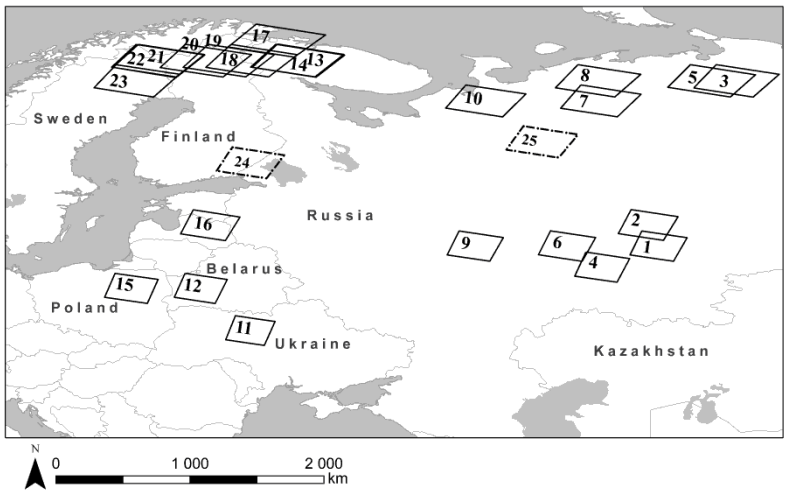

Figure 2-1. Study area of Finland and northern and eastern Europe, also indicating the locations of Landsat/ETM+ scenes employed in the validations, from **[P4]**.

2.2 Ground reference data

Snow course data

Ground reference data feasible for evaluation of fractional snow cover retrievals is often relatively difficult to obtain. This is because FSC is typically registered by human observers. Moreover, fractional snow typically varies rather widely in space and time, and therefore single point observations are not necessarily representative of the local spatial variation. This representation also depends on the landscape character and other prevailing conditions. The observations should be conducted over an area corresponding to the pixel size of the applied satellite sensor, and the timing should match the satellite overpass at least so that no major changes in snow cover occur (e.g. Hall and Riggs, 2007). The snow course network governed by the Finnish Environment Institute (SYKE) has a heritage from the beginning of the 20th century. The network consists of ~160 courses which are visited on a monthly basis. A snow course is a 2-4 km long transect passing through different landscapes; the observer registers the snow information typically at 80 locations along the transect. The observations include snow depth (SD, measured with a stick), snow density (measured with a snow tube) and fraction (%) of snow-free ground (visually estimated for an area within a 25 m radius of the observer's location). Hence, FSC=100%−Fraction of snow-free ground.

Proper *in situ* observations are particularly difficult to obtain when only trace amounts of snow are present. In a scale of a pixel, these easily remain unnoticed by human observers if only several samples are taken at ground level. The route of each snow course maintained by SYKE is individually planned so that it should represent a locality of a few square kilometers. The trail goes through different landscapes in order to catch the differences in snow conditions; the information of the prevailing landscape is assigned to each measurement location. The landscapes are: pine forest, spruce forest, mixed forest, broad-leaf forest, forest opening and open bog.

In this study, a snow course FSC mostly refers to the average value of all FSC-observations along the transect, but FSC and SD are also considered separately for open areas and forests in order to investigate the typical difference in snow conditions between these two. The analyses show that snow cover first starts decreasing in forests, but from an FSC of ~0.6 to lower snow fractions, snow ablation is faster in open areas, so that near the snow clearance there is still snow in forests when open areas are snow free (**[P4]**). Thus typically snow persists longer in forests than in open areas, although the analyses showed that the average snow depth is lower in forests (see also e.g. Golding and Swanson, 1986). Altogether, snow course measurements from the years 1991-2010 were employed in this study. The map of the Finnish snow courses and the trail of a snow course plotted over a digital photograph are shown in Fig. 2-2.

Weather station data

The weather station network of the Finnish Meteorological Institute (FMI) in Finland consists of ~250 stations, where observations on snow depth (point-wise) and snow coverage (within the range of vision) are made on a daily basis. Snow coverage is described with a particular e-code following the definitions presented by the World Meteorological Organization (WMO), see Table 2-1. The daily observations of snow coverage (e-codes) as well as the snow depths were used in this study, whenever available (observations of snow coverage were discontinued at many of the stations in 2009 due to the automation of observing protocols). Although expected to represent the average snow conditions in the locality, the snow observations may introduce a bias towards less snow than is actually present in the surrounding area, corresponding e.g. to a pixel of a satellite image. This is because each weather station is located in an open area, where snow typically disappears earlier than in forest areas, as discussed above. In order to evaluate how well the point-wise observation applies to a larger surrounding area, the correspondence between the e-code and the nearby same day's snow course FSC – providing a better spatial distribution – was analyzed and

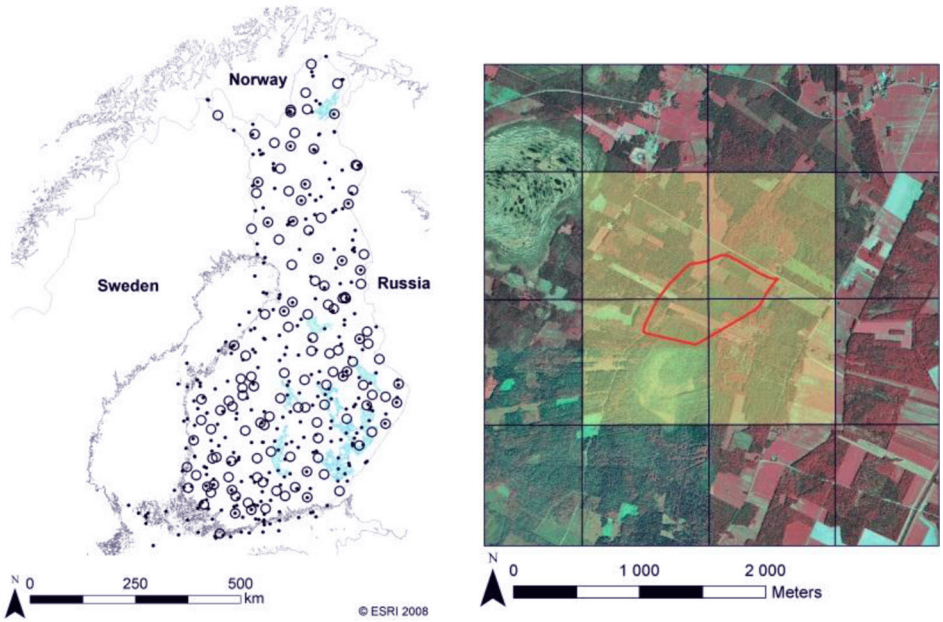

Figure 2-2. *Left:* Snow courses and weather stations of Finland. *Right:* the route of a snow course.

found to be reasonable (**[P4]**). This correspondence is considered to be an indication of spatial representativeness of point-wise observations in the scale of pixel-size of the Earth-observation imagery used in this study.

The spatial representativeness is further supported by the good correlation between snow depth observations, again from the weather stations and snow courses within a distance of <4 km for data from years 1991-2008. The correlation coefficient is 0.94, with a root mean squared (RMS) difference of 10.1 cm (see Fig. 2-3), indicating that for snow depth, point-wise observations also represent the snow conditions in a larger spatial domain.

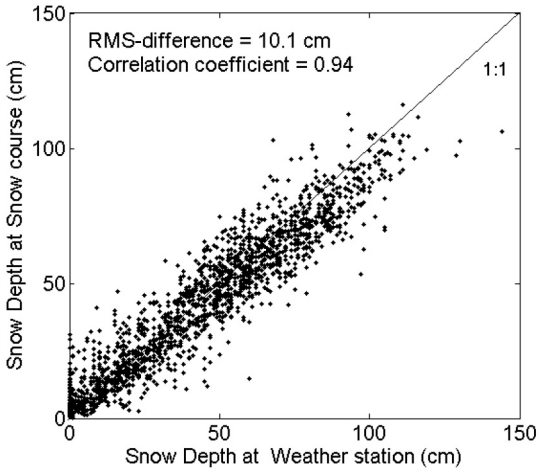

Figure 2-3. Correspondence of snow depth from weather stations and from snow courses.

Table 2-1. E-codes describing the fractional snow cover.

e-code	Indication
7,9	100% snow cover (wet and dry)
6	50% < snow cover < 100%
5	0% < snow cover < 50%
4	Open areas snow-free, snow in forests
3	0% snow cover

2.3 Earth observation data and field spectroscopy

The applied Earth Observation data are from acquisitions of 1) AVHRR (Advanced Very High Resolution Radiometer) onboard NOAA (National Oceanic and Atmospheric Administration) family of polar environmental satellites, 2) MODIS (Moderate Resolution Imaging Spectroradiometer onboard NASA EOS-Terra, 3) AATSR (Advanced Along Track Scanning Radiometer) onboard ESA/Envisat and 4) ETM+ (Enhanced Thematic Mapper +) onboard EOS Landsat-7. All data were converted to reflectances or brightness temperatures according to in-flight or pre-launch calibration information using processing software developed at the VTT Technical Research Centre of Finland.

AVHRR is a cross-track scanning radiometer measuring reflected or emitted radiation of the Earth at five (NOAA-14) or six (NOAA-15 and NOAA-16) spectral bands. These are: Band 1 (0.58-0.68 μm), Band 2 (0.725-1.0 μm), Band 3A (1.58-1.64 μm), Band 3B (3.55-3.93 μm), Band 4 (10.3-11.3 μm) and Band 5 (11.5-12.5 μm). The cross-track resolution varies from 1.1 km at nadir to 4 km at maximum scan angle (±55.4°), whereas the along track resolution is ~1 km. Given the swath width of 2600 km, NOAA/AVHRR provides a complete spatial coverage already at mid-latitudes. In this study, AVHRR data covering the years 2000-2003 were employed (**[P1]** and **[P2]**). Atmospheric correction using SMAC (Rahman and Dedieu, 1984) with an assumption of standard atmosphere was conducted to obtain surface-leaving reflectances. The data were geo-registered into a 1km×1km geographical grid in the Finnish National Coordinate system.

MODIS is a cross-track scanning instrument, which measures the Earth with 36 spectral bands from visible to thermal infrared region. The spatial resolution of the MODIS varies with the spectral band. With a scan angle of ±55°, MODIS provides a swath width of 2330 km, i.e. complete daily coverage already at mid-latitudes. In this study, the most relevant MODIS bands are Band 1 (620-670 nm), Band 2 (841-876 nm) with 250 m resolution and Band 3 (459-479 nm), Band 4 (545-565 nm) and Band 6 (1628-1652 nm) with 500 m resolution, although the thermal infrared bands Band 31 (11 μm), Band 20 (3.7 μm) and Band 32 (12 μm) with 1 km resolution also play an important role in cloud detection. However the cloud masking issues are not discussed here. The MODIS level 1B calibrated radiance data were converted into top-of-atmosphere reflectances and brightness temperatures and geo-registered into a 0.01°×0.01° WGS-84 geographical grid. Data from the year 2000-2011 were employed in this study (in **[P4]** and **[P5]**).

AATSR is a dual view, multi-channel imaging radiometer operating in seven spectral bands providing 1 km spatial resolution. Swath width is only 520 km, and therefore the complete spatial coverage at high latitudes (60º-70º) cannot be reached. The most relevant bands for this study are Band 1 (0.545-0.565 μm) and Band 4 (1.58-1.64 μm); thermal bands 5, 6 and 7 centered at 3.7 μm, 10.85 μm and 12 μm, respectively, were used for cloud masking. Data from the years 2002-2010, using only the nadir view, were used (**[P4]**). Processing followed the same procedure as for MODIS, see above.

ETM+ sensor is a whisk broom scanner which provides multispectral images at seven spectral bands (+ one panchromatic band), generally at 30 m spatial resolution. For this study, the most relevant bands are Band 2 (0.52-0.60 μm) and Band 5 (1.55-1.75 μm). Thermal bands 6 (10.40-12.50 μm) and 7 (2.09-2.35 μm) were used for cloud masking. In addition to ETM+, a few acquisitions by TM onboard Landsat-5 were also employed. All data were from 2000-2011, see **[P4]**. Processing was carried out as for MODIS and AATSR, although for the 0.00025°× 0.00025° geographical grid, close to the nominal resolution of 30 m.

MODIS snow product MOD10_L2, distributed and archived at the National Snow and Ice Data Centre (NSIDC) in Boulder, Colorado, USA, is widely used by the research community of Earth studies. The basic methods behind the product are those of Klein et al. (1998) for binary snow information and Salomonson and Appel (2004) for fractional snow information (Hall et al., 2006a; Riggs et al., 2006). In this study, the *fractional snow* in Collection 5 swath-level MOD10_L2

product (Hall et al., 2006b) was used, providing snow data in a 0.005°×0.005° grid. The data are geo-registered into a 0.01°×0.01° grid (WGS-84) in order to correspond to the processing grid of MODIS level 1B data described above.

The field spectroscopy measurements (**[P3]** and **[P5]**) were made with an Analytical Spectral Devices (ASD) Field Spec Pro JR spectrometer (ASD Inc, Boulder, Co, USA). Measurements were taken at ground level and from a 30-m high mast during the years 2007-2011. In both cases the instrument field-of-view was set to 25° so that the surface illumination area (measurement footprint) was ~20 cm in diameter for at-ground measurements and ~185 m^2 for mast-based measurements. The spectra were measured with 1.5 nm spectral resolution in the range 350-1000 nm and with 2 nm spectral resolution for 1000-2500 nm. The measured radiances were converted to Hemispherical-directional reflectance factor (HDRF) under diffuse illumination and to Bidirectional reflectance factor (BRF) under direct illumination (both referred to as *reflectance*), using a calibrated white spectralon plate as reference.

2.4 Validation techniques for fractional snow retrievals

The validation is conducted using two approaches: *absolute* and *relative*. Absolute validation refers to comparison of the obtained Fractional snow retrievals with ground truth measurements. In relative validation, Fractional snow retrievals are compared with corresponding information provided by other Earth observation sources.

As the calculation unit area varies throughout this study (from drainage basins to ~1 km pixels), the validation techniques also vary. The basic idea is to compare the FSC-estimate to the reference data considered representative for the same area. This is easy to comprehend in relative validation when pixel-to-pixel comparison is possible. The situation is more complex in absolute validation, since ground truth data are usually point-wise measurements or transect data, and the spatial representativeness of these data is not necessarily optimal. This issue is discussed in **[P4]**, where it is concluded that within acceptable accuracy, the averaged snow course FSC is representative for an area of a few square kilometers surrounding the course. The same conclusion was made for weather station observations, but the representativeness is poorer for forested landscape, as weather stations are typically located in open areas. Therefore, it is justified to compare average snow course FSC against estimate FSC from i) a 7×7 pixels window centered at the course (**[P1],** also separately for open area and forest) or from ii) pixels covering the trail of the course, as in [**P2]** and **[P4]**. When validating against the weather station data, two approaches were used in the study: iii) the basin-scale average FSC was compared with ground truth from the closest weather station located within the basin ([**P1]** and **[P2]),** and iv) the estimated FSC from one pixel overlaying the station was compared with the ground truth from the station (**[P4]**).

For areas where sufficient ground truth measurements were not available, FSC-retrievals from Landsat TM/ETM+ were used as reference, with the assumption that this FSC represents the 'truth'. Although this is not necessarily the case particularly in boreal forests, this approach is commonly used e.g. for algorithm development purposes (Salomonson and Appel, 2004; Salomonson and Appel, 2006). The methodology first classifies high-resolution TM/ETM+ pixels as 'snow' or 'not snow' using the SNOWMAP-approach of Klein et al. (1998) and then aggregates the binary data into FSC for the lower resolution pixels. In this study, binary data was provided in 0.00025° × 0.00025° resolution; then 40×40 pixels were averaged to derive FSC for 0.01° × 0.01° pixels (referred to as TM FSC hereafter) directly comparable with FSC from SCAmod (referred to as SCAmod FSC). TM FSC and SCAmod FSC were compared for each pixel where either of them identifies snow (this was in order to exclude the vast number of snow-free cases detected by both sensors, which otherwise would have dominated the results).

Comparison of estimated FSC and the reference FSC can be conducted using the original continuous values or, alternatively, the values can be categorized into certain classes and then these classes are compared. With the former approach, the differences between estimated and independent reference FSC (N cases) are analyzed using root-mean-squared-error (RMSE):

$$RMSE = \sqrt{\frac{1}{N}\sum (FSC_{estimated} - FSC_{reference})^2} \quad (2\text{-}1)$$

where $FSC_{reference}$ refers to either measured ground truth data (snow courses) or to any reference source assumed to represent the truth.

When using categorized data as from weather stations, the FSC estimates are also categorized accordingly. Then a confusion matrix is used to describe the match between predicted classes (based on estimated FSC, categorized according to the reference classes) and reference classes. For example, in the case of four classes the confusion matrix is

	True classes			
Predicted classes	**class a**	**class b**	**class c**	**class d**
class a	n_{aa}	n_{ba}	n_{ca}	n_{da}
class b	n_{ab}	n_{bb}	n_{cb}	n_{db}
class c	n_{ac}	n_{bc}	n_{cc}	n_{dc}
class d	n_{ad}	n_{bd}	n_{cd}	n_{dd}

The *total accuracy* is defined as the number of correct matches as a proportion of the total number of cases:

$$\text{Total accuracy} = (n_{aa}+n_{bb}+n_{cc}+n_{dd})/ N_{cases}, \quad (2\text{-}2)$$

where N_{cases} is the total number of cases. Accordingly,

$$\textit{Total error} = 1\text{-Total accuracy}. \quad (2\text{-}3)$$

Commission error for a class describes the proportion of estimates falling into the class which is incorrectly classified (falsely committed), e.g. for class a: $(n_{ba}+n_{ca}+n_{da})/(n_{aa}+n_{ba}+n_{ca}+n_{da})$. *Omission error* for a class describes the proportion of cases actually belonging to a class which is put into another class (falsely omitted), e.g. for class a: $(n_{ab}+n_{ac}+n_{ad})/(n_{aa}+n_{ab}+n_{ac}+n_{ad})$.

If the number of classes is reduced to two, as in the case of binary classification as ‘snow/not snow’, the success of snow identification can be expressed with *binary metrics* (e.g. Painter et al., 2009). These are *Recall* (the percentage of true snow pixels correctly predicted), *Precision* (percentage of correctly identified snow out of all pixels predicted as snow) and *Accuracy* (the ratio of correctly predicted (snow and snow-free) pixels to the total number of pixels). These were employed in **[P4]** in order to evaluate the success of SCAmod in snow identification. First, TM-derived FSC was used for labeling pixels as ‘true snow’. For the corresponding pixels, FSC from SCAmod was used to obtain ‘predicted snow’. In both cases, pixels were labeled as ‘snow’ if FSC>0.15. Finally, binary metrics were computed.

3 Results and discussion

3.1 Linear interpolation method for fractional snow cover retrieval

The retrieval of fractional snow cover was first approached with the assumption that the observed reflectance is a linear combination of reflectance of snow-covered terrain (including forest canopy) and snow-free terrain, weighted by their areal proportions:

$$\rho_{obs} = F_{snow} * \rho_{\lambda,snow} + F_{ground} * \rho_{\lambda,ground} = F_{snow} * \rho_{\lambda,snow} + (1 - F_{snow}) * \rho_{\lambda,ground} \ , \qquad (3\text{-}1)$$

where
- $\rho_{obs,\lambda}$ is the observed reflectance from the target area at wavelength λ
- F_{snow} is the areal fraction of snow-covered ground within the pixel (=FSC, Fractional Snow Cover)
- $\rho_{\lambda,snow}$ is the reflectance of snow-covered ground at wavelength λ
- F_{ground} is the areal fraction of snow-free ground within the pixel
- $\rho_{\lambda,ground}$ is the reflectance of snow-free ground at wavelength λ.

F_{snow} can be solved from (3-1):

$$F_{snow} = FSC = \frac{\rho_{obs} - \rho_{\lambda,ground}}{\rho_{\lambda,snow} - \rho_{\lambda,ground}}. \qquad (3\text{-}2)$$

Hence, having the values for reflectances from 100% snow-covered terrain and from snow-free terrain, FSC can be determined by interpolating between these two. Since these reflectances are highly dependent on local landscape characteristics, Eq. (3-1) should be applied using reflectances determined for the locality. In practice, in order to obtain FSC-estimates with a reasonable accuracy, $\rho_{\lambda,snow}$ and $\rho_{\lambda,ground}$ should be determined for each calculation unit area in the targeted region. **[P1]** describes the linear interpolation approach applicable to the boreal forest zone with a particular focus on the local determination of $\rho_{\lambda,snow}$ and $\rho_{\lambda,ground}$, referred to as *reference reflectances*. AVHRR data are used for method development, demonstrations and validation. The 1221 drainage basins (2^{nd} order division with average basin area of 320 km^2) of Finland, divided into 11 land cover categories, serve as calculation unit-areas. Accordingly, the reference reflectances are determined for each basin, and within a basin, for each land cover class separately. The Fractional snow cover is hence provided at basin-level for the 11 land cover types including open areas, forests and mixed areas, and the general FSC for a basin is determined as a weighted average of these. The reference reflectances are extracted from AVHRR reflectance time series by employing a set of dedicated rules, based on the investigated behaviour of reflectances and brightness temperatures during the snow season. A typical evolution of visible (R1) and near-infrared reflectance (R2) for forest and agricultural area is presented in Fig. 3-1, accompanied by time series of NDVI and the difference R1-R2. The importance of distinguishing between dry snow and wet snow conditions was emphasized, since using dry snow reflectance instead of wet snow would lead to underestimation of FSC. This is due to the noticeable decrease in reflectance when snow turns from dry to wet, caused by the increasing snow grain size inducing higher absorption at visible and particularly at near-infrared wavelengths (Wiscombe and Warren, 1980; Dozier et al., 1981; Nolin and Dozier, 2000; Painter et al., 2003). Since the decrease is clearly stronger at near-infrared wavelength, it is possible to identify dry snow turning to wet by observing the difference VIS-NIR (i.e. R1-R2). Whenever a sudden increase in this difference occurs, snow is considered to have turned wet, provided also that the temperature is close to 0°C. The magnitude of this change is dependent

on the land cover, predominantly on the presence of forest canopy. This is illustrated in Fig. 3-1 (bottom right), where R1-R2 is presented for forest and non-forest areas over an arbitrary basin.

Seasonally snow-covered areas are characterized by very low NDVI during the snow season, but NDVI shows a rapid increase immediately after the snow season due to the start-up of photosynthetic activity (e.g. Stow et al., 2004; Stöckli and Vidale, 2004). This is caused by an increase of visible and more pronouncedly of near-infrared reflectance. The employment of such an increased reflectance in the linear interpolation method would result in FSC overestimation. Therefore, a threshold for NDVI to identify the snow-free situation was proposed, so that if NDVI >threshold, the area is considered to be snow-free. From time-series we found that after snow clearance, the typical levels of NDVI for forest and for non-forest areas exceed 0.5 and 0.4, respectively. The former agrees well e.g. with the findings by Hall et al. (1995) and Klein et al. (1998), who observed and modeled NDVI < 0.5 for their study forests with understory snow. Hence, the proposed linear interpolation method is complemented by the NDVI-criterion with a threshold of 0.5 for forest and 0.4 for non-forest areas.

Since the methodology described in **[P1]** was implemented at the Finnish Environment Institute for operational snow mapping purposes, the study also concerned the determination of reference reflectances for basins where representative reflectance observations were not available due to the cloud cover. From the existing time series it was found that different land covers exhibit different reference values from basin to basin. This was due to the variation of landscape heterogeneity, forest density etc. Therefore, there was a need to find a measure describing the similarity between basins; then, the basin lacking the reference values could adopt them from a another basin. Assuming that forest coverage/density is the most predominant feature describing the similarity, a *Forest Sparseness Index* was developed, inspired by the previous studies on mid- and high-latitude maximum albedo by Robinson and Kukla (1985). The approach is based on the fact that the masking effect of forest canopy causes a decrease in the observed reflectance from snow-covered terrain, which is proportional to canopy density (see also e.g. Betts and Ball, 1997). Hence, to determine the forest sparseness index for each basin, AVHRR reflectance observations at full snow cover conditions were employed. Particularly the dry snow situation was considered most feasible, since wet snow exhibits a higher variability of reflectances due to the altering grain size (Dozier et al., 1981; Nolin and Dozier, 2000; Painter et al., 2003), which is not known a *priori*. Firstly, dry snow cases were identified from reflectance and brightness temperature time series, and verified with nearby weather station observations. Then, for each basin, all identified dry snow cases were averaged to obtain a final value. It was evident that theoretical dry snow reflectances could be observed only from extensive non-forested areas located mostly in northern Finland, whereas in the other parts of the country, reflectance was decreased due to forest canopy. Fig. 3-2 (left) presents the dimensionless Forest Sparseness Index for the drainage basins, scaled into a range 0 (dense forests) to 1 (open area). The reflectances as a function of Forest Sparseness Index are also presented in Fig. 3-3 for dry snow (left) and for wet snow (right). The figures illustrate how the decrease in reflectance when snow turns from dry to wet is dependent on the presence of forest canopy and how the decrease is more distinctive at near-infrared. The theoretical values for the decrease (5% for visible and ~16% for near infra-red according to Dozier et al. (1981) and Nolin and Dozier (2000)) are reached only for basins introducing only snow-cover terrain without forest canopy (i.e. high Forest Sparseness Index). This result suggests that as such, the theoretical decrease in visible and near-infrared reflectances is not applicable in discriminating between dry and wet snow, but the decrease must be proportioned to forest coverage/density.

Furthermore, some investigations of the effect of anisotropies in the observed AVHRR-reflectances were presented. From these it was concluded that due to the reflectance anisotropies of snow and forest canopy (e.g. Jin and Simpson, 1999; Cihlar et al., 1994; Warren, 1982), the linear interpolation could be applied only to reflectance data with viewing geometry close to that

which was used for determining the reference reflectance. However, these considerations are not a particular topic of this thesis.

The validation of the developed methodology for FSC retrieval was carried out using fractional snow observations from a) snow transects (snow courses) and b) weather stations as reference. Linear interpolation was applied using only VIS or both VIS and NIR (FSC computed as an average from those). When comparing against snow course data, FSC was categorized into six classes in the range 0-100%, see Fig. 3-2 for an example. For open areas, ~90% of the cases were correctly classified, whereas for forests the corresponding percentage was ~75%. These were achieved when using both VIS and NIR reflectance in the estimation. Using only VIS gave a slightly poorer result, particularly at low snow fractions. This was considered to be due to a deeper penetration depth of visible light into the snowpack, which easily leads to underestimation of FSC when the underlying ground contributes to the observed reflectance (e.g. Warren, 1982). Therefore employing NIR compensates this effect.

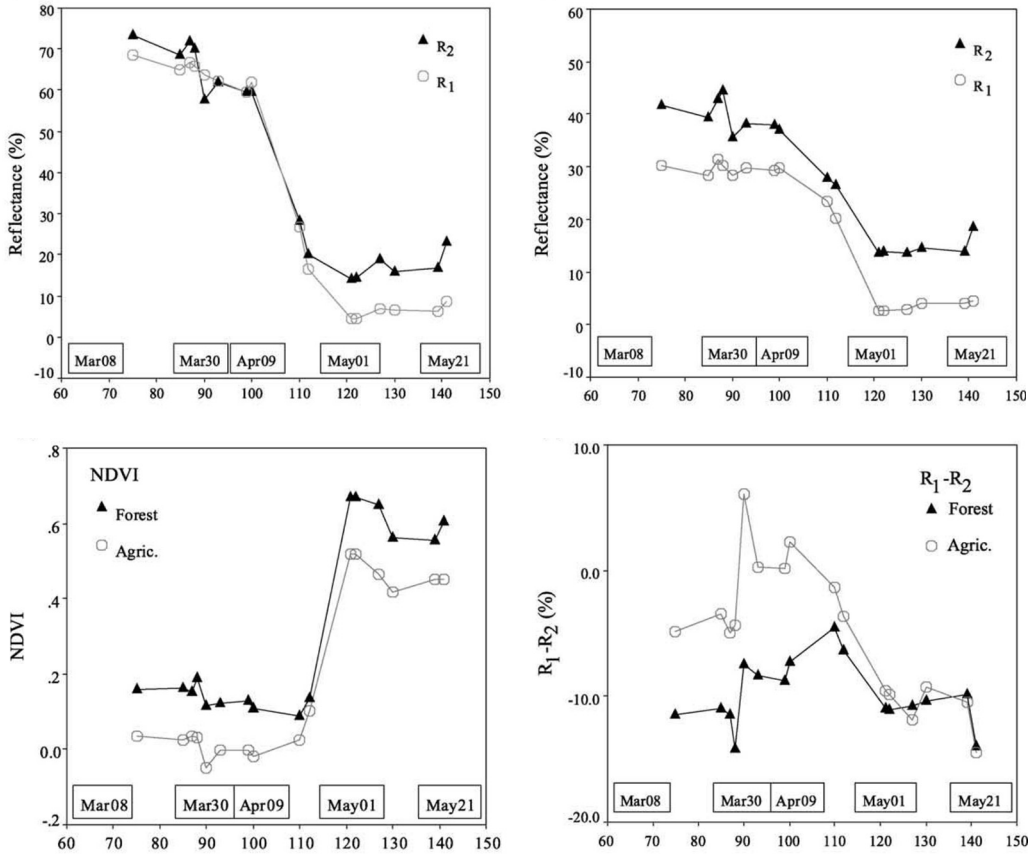

Figure 3-1. Time series of AVHRR visible (R_1) and near-infrared (R_2) reflectances as well as NDVI for an arbitrary basin, separately for open areas (agricultural) and forests (from **[PI]**).

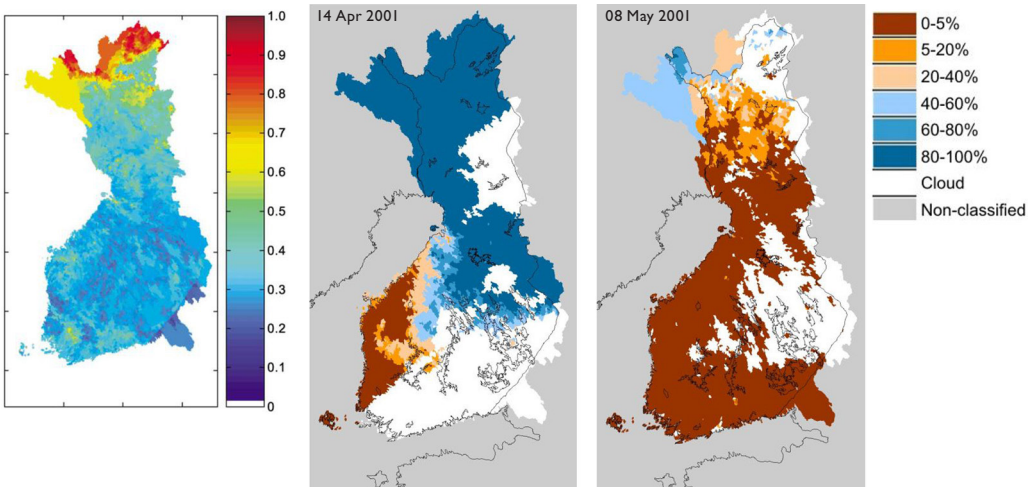

Figure 3-2. *Left:* Forest Sparseness Indices for 1221 Finnish drainage basins, from **[PI]**. *Middle and Right:* Examples of Fractional snow cover retrievals for 1221 drainage basins in Finland.

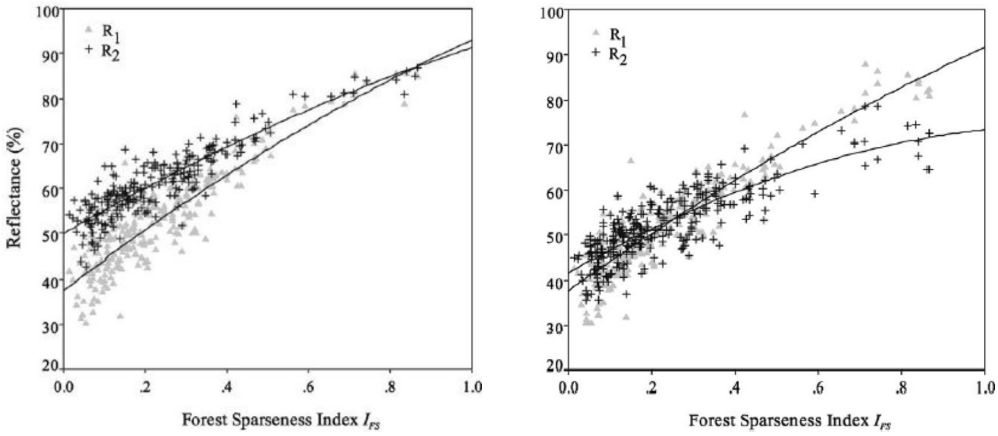

Figure 3-3. AVHRR visible (R_1) and near-infrared (R_2) reflectances from open area pixels from drainage basins representing different Forest Sparseness Indices with dry snow cover (*Left*) and with wet snow cover (*Right*), from **[PI].** Solid lines represent cubic fit curves, and are used for visualization.

3.2 The SCAmod reflectance-model based approach for fractional snow cover retrieval

3.2.1 Principles

Encouraged by the evident feasibility of Forest sparseness index in describing the forest coverage and its impact on the observed reflectance from snow-covered ground, work towards an improved modeling and consideration of forest canopy effect was started. The goal was to advance towards a physically based approach employing the radiative transfer theory. This would allow the model

parameterization using physical quantities, and would therefore leave space for further model developments based on measuring and/or modeling of these quantities, i.e. reflectances.

After reaching the upper canopy layer, the incoming radiation penetrates through the forest canopy, reaches the ground layer, reflects from it, and again penetrates through the canopy on its way back to the sensor. While passing twice through the canopy, part of the radiation is attenuated by the canopy, i.e. only a residual part is transmitted. This effect is described by *two-way transmissivity.* Transmissivity is expressed in the range 0-1, so that 1 refers to total transmission with no attenuation and 0 refers to total extinction when nothing is transmitted. The former is characterized by a non-forested target offering full view to the ground from above, whereas the latter is related to canopy so dense that the view to the ground is totally blocked. Assuming that the reflected light from a target scene is the sum of three major reflective constituents: snow, snow-free ground and tree canopy above the snow surface layer, we can formulate a reflectance model as follows:

$$\rho_{\lambda,obs}(FSC) = \overbrace{(1-t_\lambda^2)*\rho_{\lambda,forest}}^{\text{Volume scattering}} + \overbrace{t_\lambda^2*\left[FSC*\rho_{\lambda,snow}+(1-FSC)*\rho_{\lambda,ground}\right]}^{\text{Surface scattering}}, \qquad (3\text{-}3)$$

where $\rho_{\lambda,snow}$, $\rho_{\lambda,ground}$ and $\rho_{\lambda,forest}$ are the reflectances of snow, snow-free ground and (opaque) forest canopy, respectively, at wavelength λ. $\rho_{\lambda,obs}$ represents the observed reflectance from the calculation unit area. t_λ^2 represents the apparent effective two-way transmissivity for the unit area.

The model was first proposed in **[P2].** According to the model, the reflectance from the ground layer (surface scattering part of the formula) is a linear combination of snow and snow-free ground reflectances weighted by their areal proportions, with only a part of the light transmitted through the canopy. Two-way transmissivity describes the transmission of both incoming and outgoing radiation, without consideration of direction. The volume scattering part describes the reflectance of the forest canopy as a function of transmissivity. The multiplier $(1- t_\lambda^2)$ is based on the zero-order solution of the radiative transfer model (see Appendix I) with the assumption of single scattering from randomly distributed scatterers (needles, branches) inside the canopy. The idea was originally derived from the forest modeling approach by Pulliainen et al. (1994) and also coincides with studies e.g. by Schlerf and Atzberger (2006).

[P2] describes the model principles and presents its use for fractional snow cover estimation at the level of a Finnish drainage basin. Given that the transmissivity for a calculation unit area is known, FSC is determined from Eq. 3-3:

$$FSC = \frac{\frac{1}{t_\lambda^2}*\rho_{\lambda,obs} + (1-\frac{1}{t_\lambda^2})*\rho_{\lambda,forest} - \rho_{\lambda,ground}}{\rho_{\lambda,snow} - \rho_{\lambda,ground}}. \qquad (3\text{-}4)$$

Hence, the model accounts for the effect of forest canopy in the observed reflectance, provided that *a priori* information on canopy transmissivity is available. This is the challenge of using the model − but the solution is provided by the model itself. Namely, according to Eq. (3-3), if the ground layer is 100% snow covered (i.e. FSC=1), the observed reflectance originates only from the forest canopy and snow. Consequently, transmissivity can be solved from the observed reflectance as follows:

$$t_\lambda^{\,2} = \frac{\rho_{\lambda,obs}(FSC=1) - \rho_{\lambda,forest}}{\rho_{\lambda,snow} - \rho_{\lambda,forest}}, \tag{3-5}$$

given that the reflectances of forest canopy and snow are known. In **[P2]** and **[P4]** the proposed solution is to use pre-determined, generally applicable reflectances which are feasible for the target area. These can be derived from at-ground measured reflectance spectra or from Earth Observation data acquired from representative targets (e.g. for snow reflectance, non-forested areas totally covered with snow). Since dry snow has a higher reflectance than wet snow and thus exhibits a stronger contrast to the low-reflective forest canopy, it is advantageous to employ dry snow reflectance in transmissivity determination. Moreover, dry snow has a small grain size and therefore exhibits smaller reflectance variation than wet snow (e.g. Jin and Simpson, 1999; Dozier et al., 1981; Peltoniemi et al., 2005). Accordingly, the obtained transmissivities should be more insensitive to the applied viewing geometries. Thus in Eq. 3-5 $\rho_{\lambda,snow}$ and $\rho_{\lambda,obs}$ refer to dry snow. The whole approach was named *SCAmod*, which naming is used hereafter.

3.2.2 Implementation to AVHRR

SCAmod was first implemented to use NOAA/AVHRR reflectance observations at visible Band 1 580-680nm (**[P2]**). The Finnish drainage basins (5845 3rd order sub-basins with a 60 km^2 area on average) were used as calculation unit areas. The visible band was preferred over near-infrared, as in the visible region the effect of snow grain size – which *a priori* cannot be known – on the reflectance is smaller (e.g. Dozier et al., 1981; Warren 1982; Wiscombe and Warren, 1980). Snow impurities also affect the reflectance, but this concerns the visible region up to 1.0 μm (Warren, 1982) and therefore does not favour either of bands 1 and 2 of the AVHRR: the effect is slightly stronger for Band 1 but rather low when compared to the effect of grain size for Band 2.

The feasible values for the reflectance contributors were determined from AVHRR reflectances acquired under appropriate prevailing conditions (at full dry snow cover and full wet snow cover for $\rho_{\lambda,snow}$ and immediately after snow clearance for $\rho_{\lambda,forest}$ and $\rho_{\lambda,ground}$). After sampling the AVHRR-data, the representative value for each contributor was determined as an average of the samples. Variance of reflectances was also computed for each contributor (S^2_{snow}, S^2_{forest} and S^2_{ground} for wet snow, forest canopy and snow-free ground, respectively). These standard deviations were employed by statistical accuracy assessment of SCAmod, described later in this section. The basin transmissivities were generated from 15 AVHRR-scenes so that all clear-sky observations (dry snow prevailing) for each basin were used to obtain average basin reflectance, which was then used in Eq. 3-5. Due to the reflectance anisotropy of snow and forest canopy, several AVHRR-acquisitions representing a variety of different viewing and illumination geometries (nadir view, backscatter and forward scatter) were employed in determining each basin transmissivity. The average basin scale variance was also computed for statistical accuracy assessments. The resulting transmissivity map for 5845 basins is shown in Fig. 3-4.

Snow clearance shows up as a strongly decreased value for NDSI, which is therefore a useful measure when detecting the presence of snow (Hall et al., 1995, Klein et al., 1998). Nevertheless, in **[P2]**, NDVI was still proposed to be used in detecting the snow clearance, encouraged by the good experience from NDVI-thresholding (see the previous section) and also by results from other studies, e.g. by Stow et al. (2004). However, the threshold was now determined as proportional to the transmissivity. This was based on the fact that denser forests introduce higher NDVI than non-forested areas (Klein et al., 1998; Stöckli and Vidale, 2004). A linear fit between NDVI observed at snow clearance (according to reflectance time series and ground truth data from weather stations) and the transmissivity was found, see Fig. 7 in **[P2]**. Later, the original fit line was de-

creased to make the threshold more effective in catching the snow-free cases. The NDVI-rule is as follows: IF NDVI>$a \cdot t^2$+b, then FSC=0.

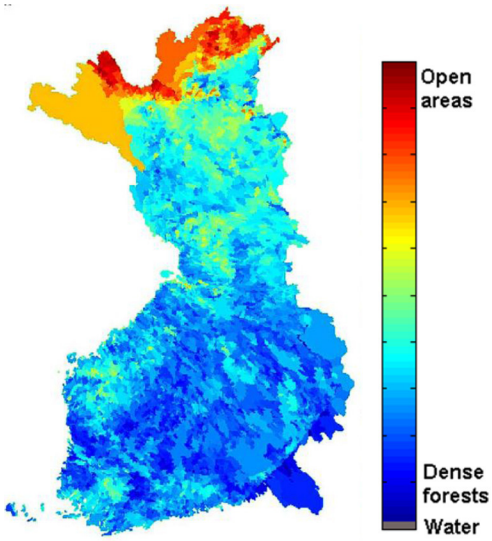

Figure 3-4.Two-way transmissivity map for 5845 Finnish drainage basins (from **[P2]**). Transmissivity range is 0.19 (basins dominated by dense forests) to 1 (open areas).

The combined use of Eq. 3-4 and the NDVI-thresholding for AVHRR-data yielded basin-scale FSC-estimates (**[P2]**), which were then compared against the ground truth data. When comparing against the weather station data, approach *iii*) as described in Section 2.4 was used. The estimates were categorized into 12 classes in the range 0-1 and compared against the four categories reported at weather stations (**[P2]**, Table 4). The resulting 1310 comparison pairs showed the best agreement for full snow cover (FSC=1) and snow-free conditions (FSC=0), as the percentage of correct predictions was 94% in both cases. Between these extremes, the FSC showed lower matching percentages ranging from 27% to 64%, depending on the category. With fractional snow, however, the results indicated that the performance of SCAmod could be better than it appears to be: for example for 0.1<FSC<0.2, weather stations showed a snow-free situation for 64% of the cases whereas only 27% were reported to have snow coverage between 0 and 0.5, which is the 'correct' category. It was concluded that these small traces of snow can really exist in the basin area particularly in forests (see **[P4]** for a more detailed analysis on spatial representativeness of weather station data), but are not observed at the weather station. The validation with the same data set is here repeated using only four categories corresponding to those used with weather station data; this allows the use of the confusion matrix as described in Section 2.4 and the result is then comparable with later results presented in **[P4]**. The new result with four categories is presented in Table 3-1. Again the results indicate that full snow cover is best identified, with an omission error of only 8.2 %. For snow-free cases, the omission error is 48.4 %, as most cases are predicted to the category representing partial snow (<50% coverage), although this might be quite correct as described above. The two fractional snow categories have omission errors of <40%. The total error rate is 24.7%, i.e. total accuracy is 75.3%.

When validating against snow course observations, approach *ii*) as described in Section 2.4 was used; thus each FSC estimate is computed as an average from pixels overlaying the course and then compared to the average FSC observed at the course. One day's time difference between AVHRR-acquisition and snow-course observation was accepted to ensure an adequate number of pairs (i.e. at least one pair in each interval of 0.2), 215 altogether. An RMSE of 0.15 in the FSC

range 0-1 was obtained, which is in line with the results from statistical accuracy analyses, also presented in **[P2]**. In addition, the accuracy was considered to be appropriate for the needs of hydrological modeling for Finnish watersheds; the use of FSC-retrievals to improve the hydrological forecasts was demonstrated for an arbitrary basin. The result indicated that FSC from SCAmod has potential to improve the discharge forecasts.

Table 3-1. FSC from SCAmod applied to AVHRR, compared to ground truth data from the weather stations.

	In situ data from weather stations					
SCAmod	**FSC=0 Snow-free ground (e-code 3)**	**0<FSC<0.5 Partial snow (e-code 4 or 5)**	**0.5≤FSC<1 Partial snow (e-code 6)**	**FSC=1 Full snow cover (e-code 7 or 9)**	**Number of estimates**	**Commission error**
FSC=0	**188**	8	4	0	**200**	6.0 %
0<FSC<0.5	176	**43**	15	2	**236**	81.8 %
0.5≤FSC<1	0	19	**95**	57	**171**	44.4 %
FSC=1	0	0	42	**661**	**703**	6.0 %
N of *in situ* cases	**364**	**70**	**156**	**720**	**1310**	
Omission error	48.4 %	38.6 %	39.1 %	8.2 %		**error rate 24.7 %**

3.2.3 Implementation to MODIS and AATSR

Soon after the first implementations and operating with the AVHRR-data covering Finland, the application area of SCAmod was extended to cover the Baltic Sea drainage basin. It was also decided to provide sub-pixel FSC instead of basin-scale FSC, in order to capture the spatial distribution of snow within basins. These improvements were implemented for MODIS-data, providing a better spatial resolution and more suitable bands for cloud screening than the AVHRR. Band 4 was considered to be the most feasible for implementations, as discussed later in Section 3.3.

The issues related to switching from AVHRR to MODIS were 1) determination of feasible values for top-of-atmosphere observed $\rho_{\lambda,snow}$, $\rho_{\lambda,ground}$ and $\rho_{\lambda,forest}$, 2) generation of a new transmissivity map employing MODIS Band 4 instead of AVHRR Band 1, as by its definition, transmissivity is wavelength-dependent and 3) employment of NDSI instead of NDVI in verifying the snow-free situation.

The values for three reflectance constituents were first derived from MODIS-data representing the suitable prevailing conditions, following the procedure described above for AVHRR but now for pixels instead of drainage basins. Later, at-ground spectral measurements provided more data for determining the values (**[P4]**).

The first MODIS-derived transmissivity map was generated using several MODIS-acquisitions from several years and underwent a series of updates later, with the aim of obtaining a complete dataset representing a wide variety of viewing and illumination angles for the needs of proper accuracy assessment. The most recent transmissivity map with a resolution of $0.01° \times 0.01°$ for Finland and its surroundings (a subset of the Baltic Sea drainage area map) is presented in Fig. 3-5. For each pixel of this map, the number of employed observations was six on average; the number ranges from 4 to 18. Statistical features related to the pixel-wise variability of the employed MODIS-reflectances and the corresponding illumination/viewing geometries are given in **[P4].** For example, standard deviation of view zenith angles (ranging from 50° backscatter to 50° forward scatter) for each pixel was determined; on average, the pixel-wise standard deviation was 27°.

In order to evaluate the effect of varying view and illumination geometries, standard deviation of Band 4 reflectance for each pixel was determined and converted to the coefficient of variation (standard deviation / average × 100%). It was found that the coefficient of variation decreases with increasing pixel-wise average reflectance, indicating that dark targets (forests) are more sensitive to the varying viewing geometry than open areas providing a higher reflectance. This finding is well in line with results e.g. by Xin et al. (2012) and corresponds to the spectral measurements in **[P5]**. The mean value for coefficient of variation was 5.7 %.

The NDSI-rule is based on the fact that low values are observed under snow-free conditions, as discussed earlier. Therefore it is in principle possible to determine a threshold to identify the snow-free situation: FSC=0 if NDSI > $NDSI_{threshold}$. The value 0.4 (or 0.1 for forested areas) as proposed by Klein et al. (1998) is however not feasible for SCAmod purposes, as the intention is to identify even small snow fractions accurately, without too conservative thresholding. Therefore it was first proposed in **[P4]** to use as low a value as -0.1 in thresholding.

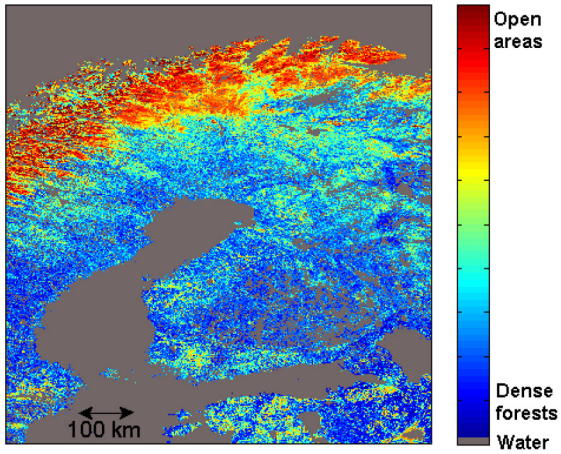

Figure 3-5.Two-way transmissivity map (t^2, range 0-1) in 0.01° × 0.01° resolution (from **[P4]**).

Applying SCAmod to AATSR data after experiences with MODIS was rather straightforward, as AATSR Band 1 measures reflectance at the same wavelengths as MODIS Band 4. Therefore, $\rho_{\lambda,snow}$, $\rho_{\lambda,ground}$ and $\rho_{\lambda,forest}$ determined for MODIS are also considered to be feasible when using AATSR data. Moreover, derivation of the transmissivity map from AATSR observations would be complicated due to the limited geographical coverage (a few days' gaps in AATSR acquisitions would drastically reduce the number of suitable observations). Hence, the transmissivity from MODIS was employed when applying SCAmod to AATSR.

Validation of FSC-retrievals against Finnish weather station data were conducted using 1745 data pairs. In comparisons, the estimated FSC for one pixel overlaying the station is compared with the concurrent (same day) snow coverage information given by the e-code, i.e. approach *iv*) as described in Section 2.4. The same comparison was also made for MOD10_L2 FSC, categorized accordingly. The general performances of SCAmod applied to AATSR ($SCAmod_{AATSR}$) and to MODIS ($SCAmod_{MODIS}$) were rather similar: the overall accuracy was 65.1 % for $SCAmod_{AATSR}$ and 65.9 % for $SCAmod_{MODIS}$.

Full snow cover is well identified by SCAmod, but MOD10_L2 shows underestimation: ~60 % of full snow cover cases are omitted. MOD10_L2 also shows frequent underestimations for partial snow cover: e.g. for true 0≤FSC<0.5, 65% is falsely interpreted as snow-free. The corresponding percentages with SCAmod were 33% (MODIS) and 40% (AATSR). The underestimation problem with MOD10_L2 is probably due to the presence of forest within the snow course, as this is known to lead to poorer performance, particularly to underestimations (Hall and Riggs, 2007; Salomon-

son and Appel, 2004; Rittger et al., 2012). Snow-free ground was well recognized by all three products with an omission error ranging from 1.3% to 19.3%. The overall accuracy was 65.1% for $SCAmod_{AATSR}$ and 65.9% for $SCAmod_{MODIS}$, whereas the overall accuracy for MOD10_L2 was 46.4%. Therefore it was concluded that SCAmod provides a better performance than MOD10_L2 FSC, whether using MODIS or AATSR.

Validation against snow course data reveals similar results as with AVHRR. The obtained RMSE (range 0-1) for 44 cases were 0.12 and 0.14 with MODIS and AATSR, respectively, whereas MOD10_L2 showed an RMSE of 0.20, mostly due to underestimations. Exclusion of cases with true FSC=1 provides better information on accuracy particularly for fractional snow: the RMSEs in this case were 0.15 (MODIS), 0.14 (AATSR) and 0.21 (MOD10_L2).

As SCAmod was specifically developed to perform well in boreal forests, it was interesting to evaluate whether the accuracy of FSC estimation depends on the canopy transmissivity, related to canopy obscurance. Testing this was accomplished using MODIS-acquisitions from full snow cover conditions; any deviation from FSC=1 was treated as an underestimation. The data set includes FSC-estimates for 7×7 pixel windows (~ 7×7 km^2) centered at weather stations reporting full snow cover (again with the assumption that the weather station observation is valid for this larger area). RMSE was computed for $FSC_{reference}$=1. The result for SCAmod and MOD10_L2 fractional product is presented in Fig. 3-6. It is obvious that SCAmod underestimations are not distinctively correlated with transmissivity, whereas MOD10_L2 shows stronger and more frequent underestimations towards low transmissivity, i.e. towards dense forests. The results for MOD10_L2 agree well e.g. with those of Hall et al. (2007), Rittger et al. (2012) and Salomonson and Appel (2004).

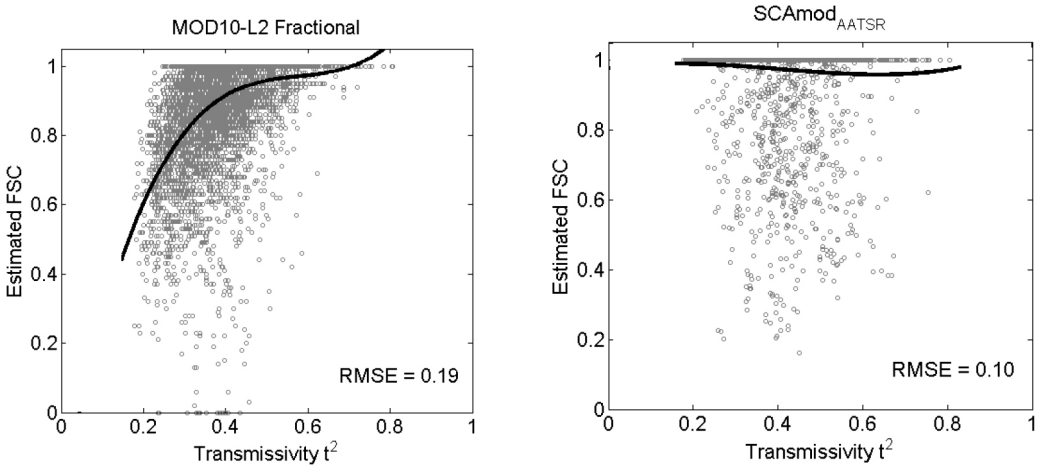

Figure 3-6. Underestimations of true 100 % snow cover with *Left*: MOD10_L2 fractional product and *Right:* $SCAmod_{AATSR}$. The bold curve represents a cubic fit to visualize the dependence of underestimations on the transmissivity, from **[P4]**.

3.2.4 Statistical accuracy

The performance of SCAmod is strongly dependent on the local representativeness of the reflectance contributors. The reflectance from snow, forest canopy and snow-free areas vary by nature, but in this study, generally feasible average values are used as described above. Assuming that the average values are representative for the target geographical area, it is however possible to estimate the error in FSC retrieval, based on the variability (standard deviation) of the applied reflectances. The *statistical accuracy* of SCAmod FSC can be derived from Eq. (3-4) using the law of error propagation (e.g. Taylor, 1982), which gives the variance for FSC (S^2_{FSC}) as follows:

$$S^2_{FSC}(\rho_{\lambda,obs}(FSC),t) = \tag{3-6}$$

$$\left(\frac{\partial F}{\partial \rho_{\lambda,obs}(FSC)}\right)^2 S^2_{obs} + \left(\frac{\partial F}{\partial t}\right)^2 S^2_t + \left(\frac{\partial F}{\partial \rho_{snow}}\right)^2 S^2_{snow} + \left(\frac{\partial F}{\partial_{forest}}\right)^2 S^2_{forest} + \left(\frac{\partial F}{\partial \rho_{ground}}\right)^2 S^2_{ground},$$

where F is the function giving FSC (Eq. 3-4). S^2_{obs} is the variance of observed reflectance and S^2_t is the variance of transmissivity. S^2_{snow}, S^2_{forest} and S^2_{ground} are the variances for wet snow, forest canopy and snow-free ground reflectance, respectively, here determined empirically from Earth Observation data as described above. In **[P2]**, the derivation of final formulae for S^2_{FSC} is described in more detail; the result is given in the following:

$$\begin{aligned}
&S^2_{FSC}(\rho_{\lambda,obs}(FSC),t) = \\
&\left(\frac{\frac{1}{t^2}}{\rho_{snow}-\rho_{ground}}\right)^2 S^2_{obs} + \left(\frac{2(\rho_{forest}-\rho_{\lambda,obs}(FSC))/(\rho_{snow}-\rho_{ground})}{t^3}\right)^2 S^2_t + \\
&\left(-\frac{\frac{1}{t^2}\rho_{\lambda,obs}(FSC)+(1-\frac{1}{t^2})\rho_{forest}-\rho_{ground}}{(\rho_{snow}-\rho_{ground})^2}\right)^2 S^2_{snow} + \\
&\left(\frac{1-\frac{1}{t^2}}{\rho_{snow}-\rho_{ground}}\right)^2 S^2_{forest} + \left(\frac{\frac{1}{t^2}\rho_{\lambda,obs}(FSC)+(1-\frac{1}{t^2})\rho_{forest}-\rho_{snow}}{(\rho_{snow}-\rho_{ground})^2}\right)^2 S^2_{ground}.
\end{aligned} \tag{3-7}$$

Accordingly, having a reflectance observation $\rho_{\lambda,obs}$ from a unit-area with a certain FSC and transmissivity t, the variance of the estimated FSC can be determined. A more usual measure is standard deviation (standard error in a non-biased case), $\text{std}_{FSC} = \sqrt{S^2_{FSC}}$. The standard deviation is also used to determine the confidence limits for an FSC-estimate; e.g. 95% confidence limits are determined as FSC±2·std_{FSC}, given that the number of cases is large and that the error is normally distributed. Since the statistical accuracy varies according to the transmissivity and the FSC-level, Eq. 3-7 is useful in simulation of the accuracy of SCAmod FSC in general and helps in evaluation of the influence of the model parameterization on the final outcome. Standard deviation of FSC as

a function of standard deviation of wet snow reflectance ($\sqrt{S^2_{snow}}$) is presented in Fig. 3-7. In this particular simulation, $\rho_{\lambda,drysnow}$, $\rho_{\lambda,snow}$, $\rho_{\lambda,forest}$ and $\rho_{\lambda,ground}$ are determined as discussed in **[P3]**, **[P4]** and **[P5]**, and correspond to MODIS top-of-atmosphere reflectances. In order to simulate the effect of S^2_{snow} only, S^2_{forest} and S^2_{ground} were set to zero. It can be seen that the standard deviation of FSC increases strongly (i.e. the accuracy weakens) towards higher values of S^2_{snow}. The accuracy is weakest for high FSC, simply because in that case the wet snow reflectance dominates the observed scene reflectance. The efforts towards finding representative values for S^2_{snow}, S^2_{forest} and S^2_{ground} as well as for, $\rho_{\lambda,drysnow}$, $\rho_{\lambda,snow}$, $\rho_{\lambda,forest}$ and $\rho_{\lambda,ground}$, and their implications for SCAmod performance are described in Section 3.3.

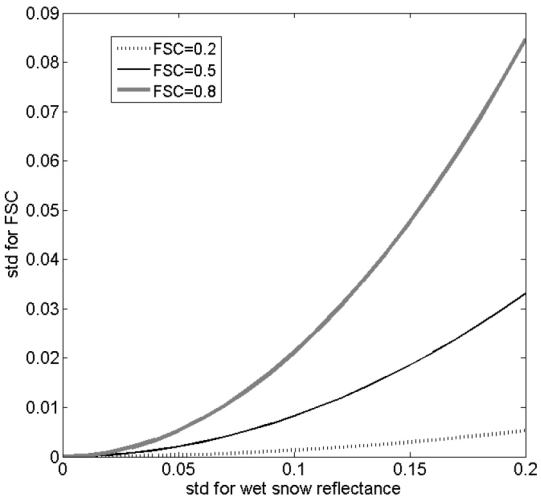

Figure 3-7. The modeled standard deviation (standard error) of FSC as a function of wet snow reflectance fluctuations.

3.3 Field spectroscopy measurements for SCAmod development

As discussed in Section 3.2, the variability of the reflectances affects the statistical accuracy of the developed methodology. However, the essence of the SCAmod performance is the validity/representativeness of the applied values for reflectances of snow, forest canopy and snow-free ground. If these parameters are non-representative, the FSC estimation shows poor results when compared to real snow conditions at ground level. Therefore, efforts have been made to find the proper values for these reflectances and at the same time, to catch their variances and particularly to identify the main reason for the variation. Investigation of spectra from the three reflectance contributors also provides suggestions on optimal wavelength bands for SCAmod: the wavelength region introducing the smallest variation is preferred as it leads to low standard deviation of the estimated FSC. It should be noted, however, that there are also other sources of error when employing Earth Observation data. A major factor is the atmosphere that reflects and absorbs the radiation, these mechanisms depending on the gaseous concentrations and aerosol contaminations as well as on the wavelength. Therefore, choosing an optimal wavelength band cannot be based only on spectral properties of the target but must also take into account more general knowledge of the atmospheric effect in different wavelengths. However, these considerations are not within the scope of this thesis.

In order to extend the understanding of the behaviour of spectra from snow and snow-free ground, spectra from tower-based and ground-based ASD field spectroscopy measurements were studied (**[P3]**). This dataset was further complemented with tower-based spectral measurements

from snow-covered forest stand and forest opening (**[P5]**). In this thesis, the results and conclusions from spectral measurements are utilized particularly in a) selection of the most suitable wavelength band to be employed by SCAmod, b) determining the most appropriate values for snow and snow-free ground reflectances for SCAmod and c) improving understanding of the behaviour of NDSI in a snow-covered forest.

[P3] discusses the differences in snow spectra caused by grain size, snow depth and wet/dry status predominantly from the point of view of SCAmod, mostly using ground-based measurements. Spectra from snow-free ground were also investigated but without consideration of vegetation type or soil properties (several understory vegetation species were observed but they were analysed as a whole). All measurements were taken under both direct and diffuse illumination in order to identify the possible significant differences between these two cases. A few selected wavelength bands corresponding to those of AVHRR and MODIS were of particular interest. These were extracted from the original spectra by averaging within the corresponding spectral range.

The reflectance spectra (average and standard deviation) from wet snow and from snow-free ground are presented in Fig. 3-8. Wet snow spectra are presented for shallow (<20 cm) and deep (>20 cm) snowpack. The spectral band-specific mean reflectances and their standard deviations were also listed in **[P3]**. It was found that standard deviations of reflectance under direct and diffuse illumination do not significantly differ in this dataset. Therefore it was concluded that these variances are predominantly due to the target characteristics, because a) the variance cannot be due to the sun zenith angle under diffuse illumination and b) the variance cannot be due to the viewing geometry only because nadir view is used.

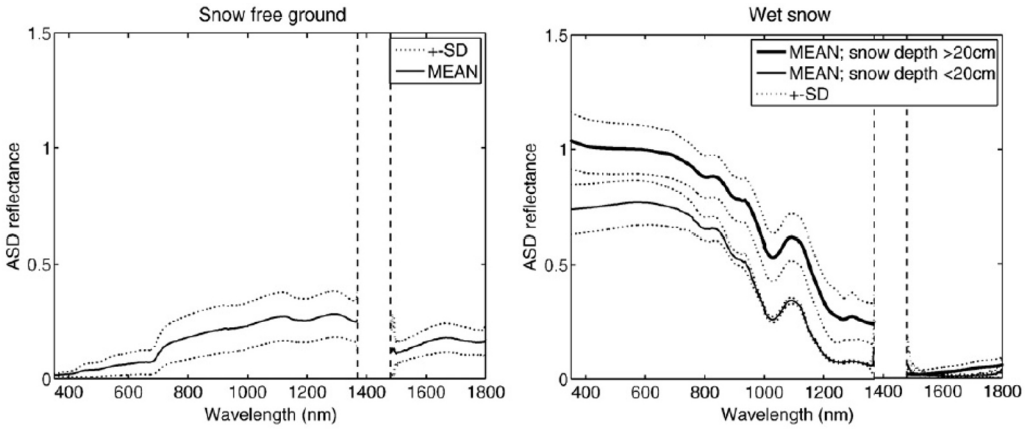

Figure 3-8. *Left*: Mean reflectance±standard deviation for snow-free ground. *Right:* Mean reflectance±standard deviation for wet snow in cases where snow depth is either above or below 20 cm. Results include both direct and diffuse illumination. The wavelength area around 1400 nm is affected by a bad signal-to-noise ratio of the applied ASD-spectrometer (from **[P3]**).

The selection of optimal channel for SCAmod can be based on the observed mean and standard deviation of wet snow, forest canopy and snow-free ground reflectance, using the law of error propagation to derive the total error, as discussed in Section 3.2. In **[P3]**, these investigations were initiated, focusing only to the contribution of wet snow and snow-free ground, i.e. simulations were made under the assumption of a non-forested area with a transmissivity of 1.

In addition to the standard deviation, *coefficient of variation* (standard deviation / mean) is a useful measure as it relates the standard deviation to the reflectance level. The standard deviations and coefficients of variation as a function of wavelength [350-1000 nm] for wet snow and

snow-free ground are presented in Fig. 3-9. For wet snow, standard deviation decreases slightly in the visible region, but the coefficient of variation increases rapidly around near-infrared. This is because at near-infrared, wet snow reflectance exhibits a strong decrease, and at the same time is more sensitive to the grain size variations (e.g. Jin and Simpson, 1999; Nolin and Dozier, 2000). For snow-free ground, standard deviation exhibits an increase at near-infrared, but at the same time the reflectance increases, causing a distinctive decrease in coefficient of variation. Considerations of these changes and their effects on optimal wavelength band selection were presented in **[P3]** but some further conclusions are presented here. It is true that the low coefficient of variation for a certain band would suggest a smaller total error, but only if the contrast between snow and snow-free ground reflectance remains high. Namely, according to SCAmod-formulae, and consequently Eq. (3-7), this contrast (the difference between wet snow reflectance and snow-free ground reflectance) strongly regulates the total error. This is demonstrated here, employing the observed means and standard deviations of wet snow and snow-free ground for spectral bands corresponding to MODIS Band 3 (blue, 459-479 nm), Band 4 (green, 545-565 nm), Band 1 (red, 620-670 nm) and Band 2 (near-infrared, 841-876 nm). Forest canopy contribution is neglected in the analysis, i.e. a non-forest case is considered. The resulting standard errors are presented in Fig. 3-10. The error is highest at near-infrared, since although exhibiting the low coefficient of standard deviation, the contrast between snow and snow-free ground reflectances is significantly smaller than at visible bands (see Fig. 3-8 for reflectance spectra).

According to Fig. 3-10, blue Band 3 shows the lowest error, but in practice its use is hampered by the particularly strong atmospheric scattering at the blue region. Since green Band 4 also exhibits a low standard error, it was concluded that Band 4 is more feasible for FSC-retrieval with SCAmod. This decision was supported by the fact that NDSI also uses Band 4 reflectance. Hence, Band 4 reflectance was employed for SCAmod fractional snow cover retrievals in **[P4]** and **[P5]**.

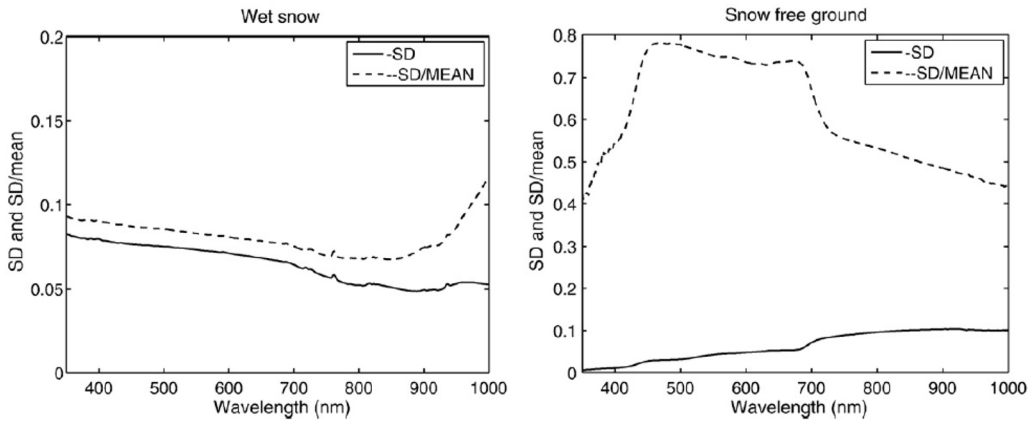

Figure 3-9. Standard deviation (range 0-1 in reflectance units) and the coefficient of variation of reflectance from ASD-measurements. *Left*: wet snow, *Right*: snow-free ground, from **[P3]**.

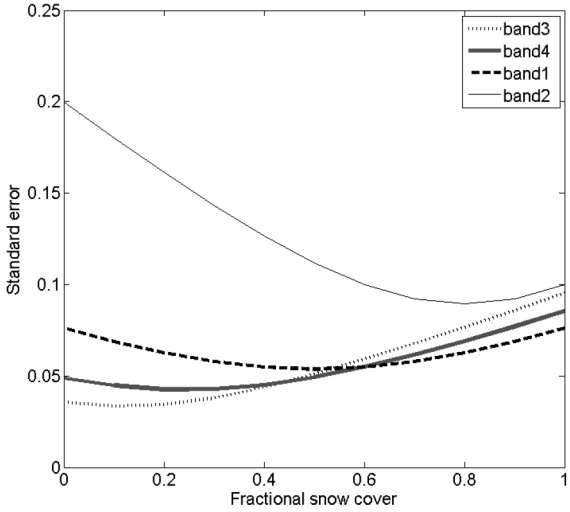

Figure 3-10. The modeled standard error (standard deviation) for FSC (range 0-1) applied to four MODIS bands, with contributions of wet snow and snow-free ground reflectance fluctuations.

[P5] aimed at a better understanding of the contribution of forest canopy to the observed scene reflectance from a snow-covered forest. This was accomplished using tower-based spectral observation from a forest stand and from a forest opening with shadows casted by surrounding trees. The sensitivities of the reflectances and their related indices (NDVI and NDSI) were investigated by conducting the spectral measurements under both direct and diffuse illumination. The basic idea with this approach is that if e.g. NDSIs under direct and diffuse illumination are congruent, then this index is not very sensitive to either illumination or viewing conditions. In such a case, the possible variance in the index must be due to the actual target characteristics such as snow grain size. It was found that for forest opening the NDSI is relatively invariant to the illumination and viewing geometry, whereas for forest stand NDSI changes with illumination and view zenith angle. This is illustrated in Fig. 3-11, where the temporal evolution of NDSI within one snow season, is presented for forest opening (Left) and for forest stand (Right) separately for direct and diffuse illumination. This result agrees with that of Xin et al. (2012), who reported a strong dependence between NDSI and view and sun geometries. It is generally known that NDSI-based methods find less snow for forests than for open areas (e.g. Rittger et al., 2012; Hall and Riggs, 2007); one aim of the study was to investigate the success of the method for the test site representing a medium-dense boreal forest.

The MODIS snow mapping method (SNOWMAP) was originally based on threshold values for NDSI as well as Band 2 and Band 4 reflectances. A pixel was classified as 'snow' if all three parameters fell within a specified acceptance region defined by the fixed thresholds. Later, an extension to the NDSI acceptance area, based on the NDVI, was added (Klein et al., 1998). This was made in order to improve the method performance in forests. The acceptance region projected to NDSI-NDVI plane is shown in Fig. 3-12 together with the corresponding samples from tower-based spectral measurements (**[P5]**). It can clearly be seen that observations from snow-covered ground are partly outside the acceptance region and would be classified as snow-free. Even with full snow cover of >40cm in depth, a major part of the observations falls outside the region. Even some negative values were observed from full snow-covered forest.

Concerning this thesis, the obtained information on the behavior of NDSI in the snow-covered forest is important. It emphasizes the strength of SCAmod compared to NDSI-based retrieval methods. An example of the performance of NDSI-based methods for a fully snow-covered scene over a dense forest area is presented in Fig. 3-13. Very low NDSI-values result in false snow commissions in binary product (by Klein et al., 1998) as well as in too low FSC in fractional snow product (by Salomonson and Appel, 2004).

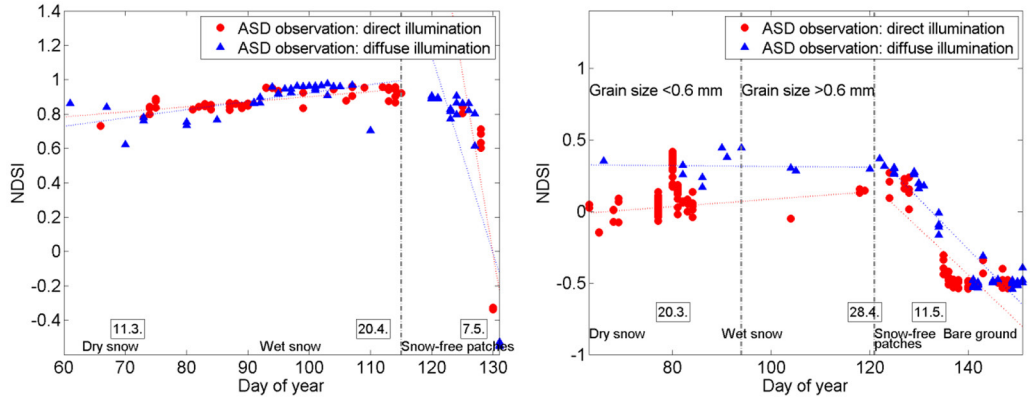

Figure 3-11. The behaviour of NDSI for *Left:* snow-covered forest opening and *Right:* snow-covered forest, from **[P5]**. The solid red and blue lines are linear fit curves (before and after the first appearance of snow-free patches indicated by the vertical dashed line), and are used for visualization.

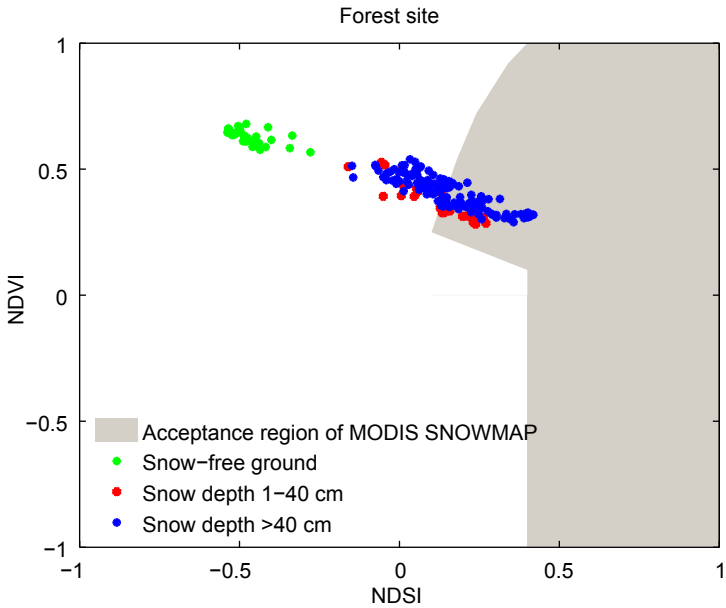

Figure 3-12. The MODIS SNOWMAP method: acceptance region projected to NDSI-NDVI-plane as defined by Klein et al. (1998), and the corresponding samples from tower-based spectral measurements, from **[P5]**.

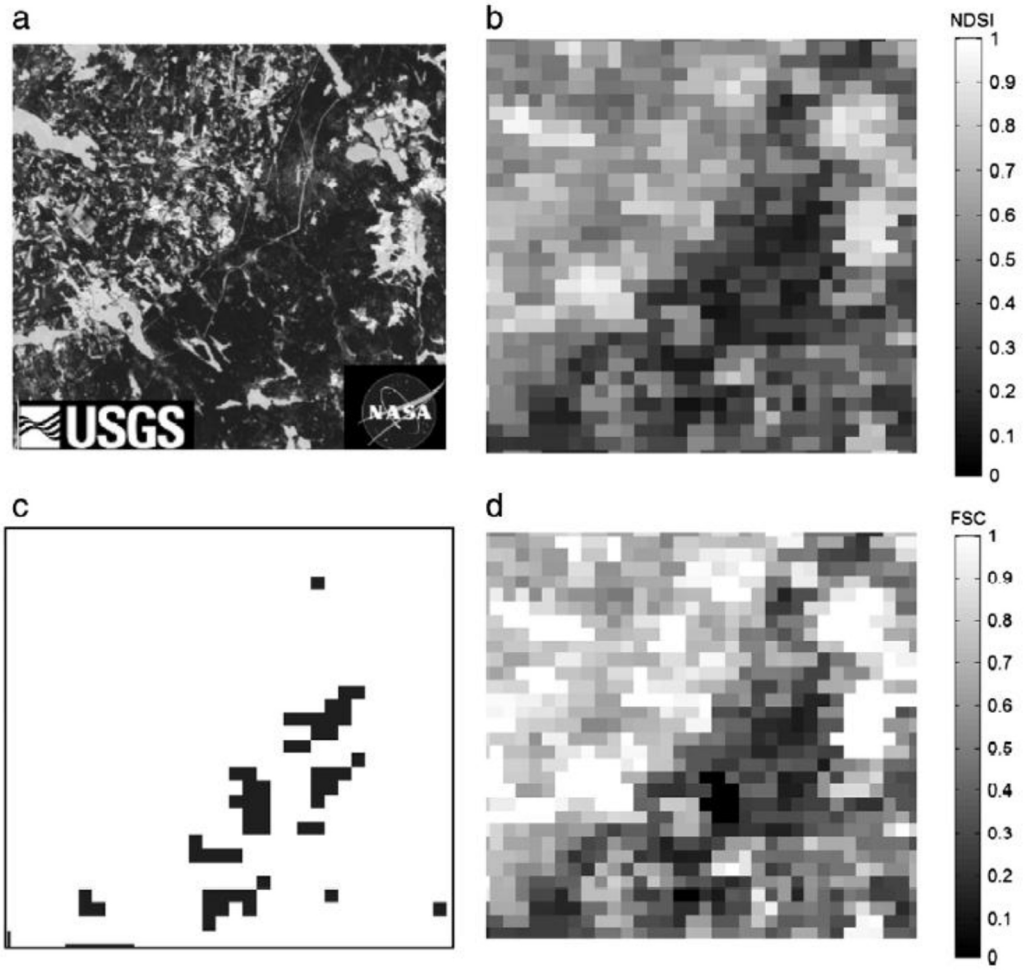

Figure 3-13.The performance of MODIS snow mapping methods over a fully snow-covered scene on 28 March 2003. a) A subset of Landsat/ETM+ scene on 15 March 2003, characterized by very dense forests, b) NDSI in MODIS 500 m-resolution, c) MOD10_L2 binary snow, white=snow, black=no snow, d) MOD10_L2 fractional snow, from **[P5]**.

3.4 Extension of the reflectance model-based approach SCAmod to continental scale

As discussed in Section 3.2.3, SCAmod was shown to provide information on fractional snow cover for Finland with a reasonable accuracy even for forest areas, with RMSE<0.15 in the FSC range 0-1. Expansion of the target area to cover the Baltic Sea drainage basin was associated with using MODIS Band 4 and moving to the sub-pixel level, as discussed earlier. The feasibility of SCAmod outside the Baltic Sea area was first demonstrated for Northern Manitoba, Canada (Anttila et al., 2006). The attempts to apply SCAmod at even larger scale were initiated within the European Space Agency (ESA) DUE-project GlobSnow (2008-2012), aiming at producing a 15-year Snow extent dataset using ERS-2/ATSR-2 and Envisat/AATSR-data (Luojus et al., 2010).

The transmissivity map can be established using reflectance data acquired under full snow cover conditions, as described in Section 3.2. However, the derivation of pixel-wise forest transmissivity was a laborious task when implementing SCAmod in the Baltic Sea drainage area, as numerous MODIS-acquisitions were needed to properly cover the entire area. In continental/hemispheric scale, this approach would be far too laborious to accomplish; therefore, a new method for generating the transmissivity also using global land cover data was developed and implemented for the northern hemisphere for the requirements of the GlobSnow-project. The approach was described and demonstrated in **[P4]** without going into detail. However, in order to evaluate the feasibility of the new method, both types of transmissivity were employed by SCAmod, followed by absolute and relative validations.

Transmissivity was first determined from MODIS-acquisitions (as described in Section 3.2) for five extensive 'teaching areas' in the northern hemisphere, together compounding an area of ~7 million km^2. For each area, transmissivity distributions (mean and standard deviation) were determined for present GlobCover-classes and then combined after normalizing with respect to the size of the teaching area. An example of distributions for two classes is presented in Fig. 3-14. It was found that in general, GlobCover classes are rather well separated with respect to their typical average transmissivity, although some classes exhibited a wide standard deviation and their distributions were overlapping. Nevertheless, it was considered reasonable to determine the continental transmissivity maps using GlobCover data and these averages. The feasibility of this approach was later verified simply by comparing the original MODIS-derived transmissivity (hereafter referred to as $trans_{MODIS}$) and the new GlobCover-derived transmissivity ($trans_{GC}$), as discussed later in this section. The transmissivity for each 0.01° × 0.01° pixel of the whole target area is expressed as a linear combination of class-wise average transmissivity and the class-wise occurrence of GlobCover pixels (4×4) falling into that pixel, as follows:

$$transmissivity_{i,j} = \sum_{c=1}^{N_{classes}(i,j)} \frac{n_{c,i,j}}{n_{tot,i,j}} * mean(trans_{MODIS}(c)), \tag{3-8}$$

where i,j are grid cell coordinates (cell size 0.01º × 0.01º)
$n_{c,i,j}$ is number of GlobCover pixels of class c within a grid cell i,j
$n_{tot,i,j}$ is the total number of GlobCover (0.0025º × 0.0025º) pixels within the grid cell i,j (=16)
$mean(trans_{MODIS}(c))$ is the mean transmissivity for class c
$N_{classes}(i,j)$ is the number of GlobCover classes within the grid cell i,j.

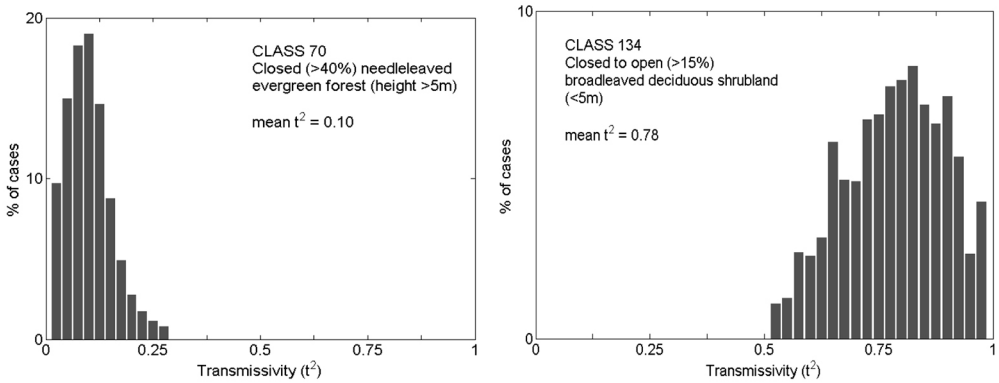

Figure 3-14. Distribution of two-way transmissivities for two samples of GlobCover classes.

The resulting GlobCover-derived two-way transmissivity map for Eurasia was introduced in **[P4]**, here presented in Fig. 3-15. For the study area of northern and eastern Europe (Fig. 2-2), where $trans_{MODIS}$ is also available for the teaching areas, FSC was provided using SCAmod with both transmissivities. This was in order to validate SCAmod performance in general and to evaluate the effect of the GlobCover-based approach on the FSC-retrievals. Since proper ground measurements of FSC were not available outside Finland, a *relative validation*, i.e. comparison against FSC from 23 Landsat TM-scenes over the study site, was conducted. Only MODIS-data with SCAmod was tested; AATSR was not employed due to a limited number of spatially and temporally coincident TM and AATSR acquisitions. *Absolute validation*, i.e. comparison against snow course observations, was also repeated both for MODIS and AATSR. **[P4]** presents the validation results in detail.

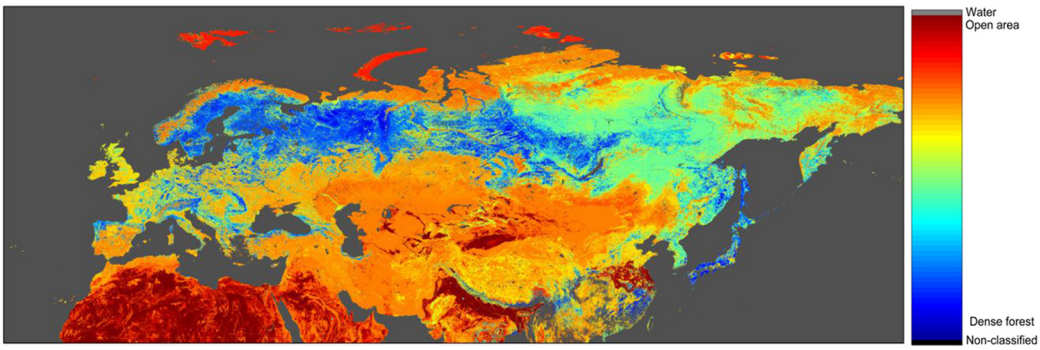

Figure 3-15. Two-way transmissivity (t^2, range 0-1) for Eurasia, derived from MODIS-based transmissivities and GlobCover-data.

Relative validation showed in principle a good correlation between SCAmod-derived FSC and TM-derived FSC, see Fig. 3-16 for three sample scenes. An average RMSE of 0.12 (range 0-1) was obtained when employing MODIS-derived transmissivity. The result is affected by the fact that TM-derived FSC often overestimates the moderate to high snow fractions while underestimating or omitting the very low snow fractions. In addition, the threshold where underestimation turns into overestimation varies according to the presence of forest (e.g. Rittger et al., 2012). In practice this can be seen as a reduced area of fractional snow by TM particularly in areas where the size and distribution of snow-free patches vary at a spatial scale finer than that of the TM-pixel. At very low snow fractions, this results in a low value for precision (pixel correctly identified as snow / all pixels identified as snow), as SCAmod identifies the low snow fractions as 'snow' whereas TM FSC does not. At higher snow fractions, still <1 (100%), the overestimations by TM do not show up in binary metrics but are seen as a higher RMSE and as an s-shape curve of the comparison scatter-plot, see Fig. 3-16 (bottom).

When employing $trans_{GC}$, the relative validation shows very minor changes in the FSC-retrievals: on average, RMSE from 23 TM-scenes decreased from 0.12 to 0.14. The results for the three arbitrary scenes are again presented in Fig. 3-17, showing the increase of RMSE for only one of the scenes. Accordingly, the binary metrics from relative validation also show only minor deterioration <1%, see Table 3-2.

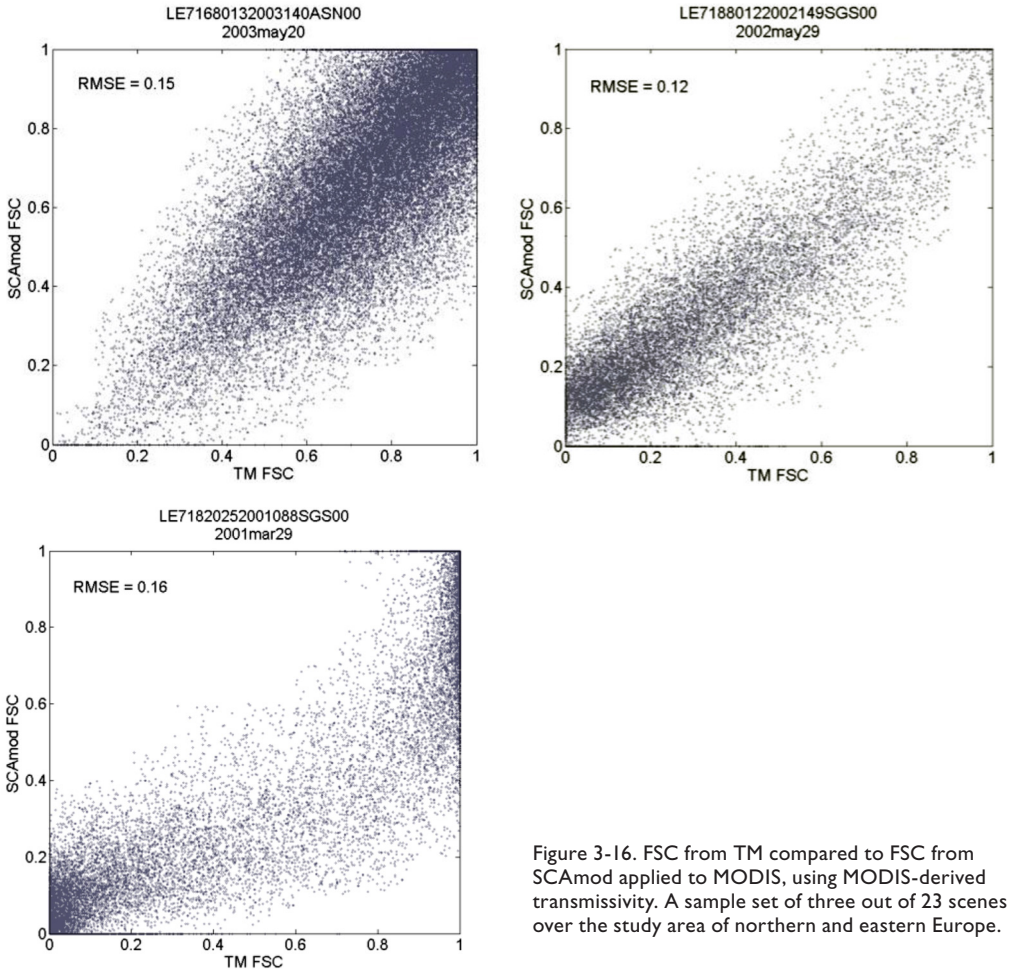

Figure 3-16. FSC from TM compared to FSC from SCAmod applied to MODIS, using MODIS-derived transmissivity. A sample set of three out of 23 scenes over the study area of northern and eastern Europe.

Table 3-2. The effect of applying GlobCover-derived transmissivity instead of MODIS-derived transmissivity in SCAmod on the obtained FSC. Binary metrics for 23 TM-scenes on average are presented (from Appendix I in **[P4]**).

	Recall %	**Accuracy %**	**Precision %**	**RMSE (range 0-1)**
Average from all scenes ($trans_{MODIS}$)	**95.64**	**96.05**	**94.48**	**0.12**
Average from all scenes ($trans_{GC}$)	**95.07**	**96.17**	**95.37**	**0.14**

The results from *absolute validation* against *in situ* snow course observations also indicate that the employment of $trans_{GC}$ decreases the FSC estimation accuracy, although only slightly. For example with MODIS, RMSE is increased from 0.11 to 0.14, see Fig. 3-18 presenting the absolute validation with $trans_{MODIS}$ (upper pane) and with $trans_{GC}$ (lower pane).

As a result of the absolute and relative validations, it was concluded that the GlobCover-based approach for transmissivity generation is a feasible method. The fact that the employed TM-reference data may exhibit biased FSC (Rittger et al., 2012) is evidently a defect, affecting the absolute error assessment. However, the results from relative validation are well in line with the results from absolute validation, which means that relative validation does give an indication of the general performance of SCAmod.

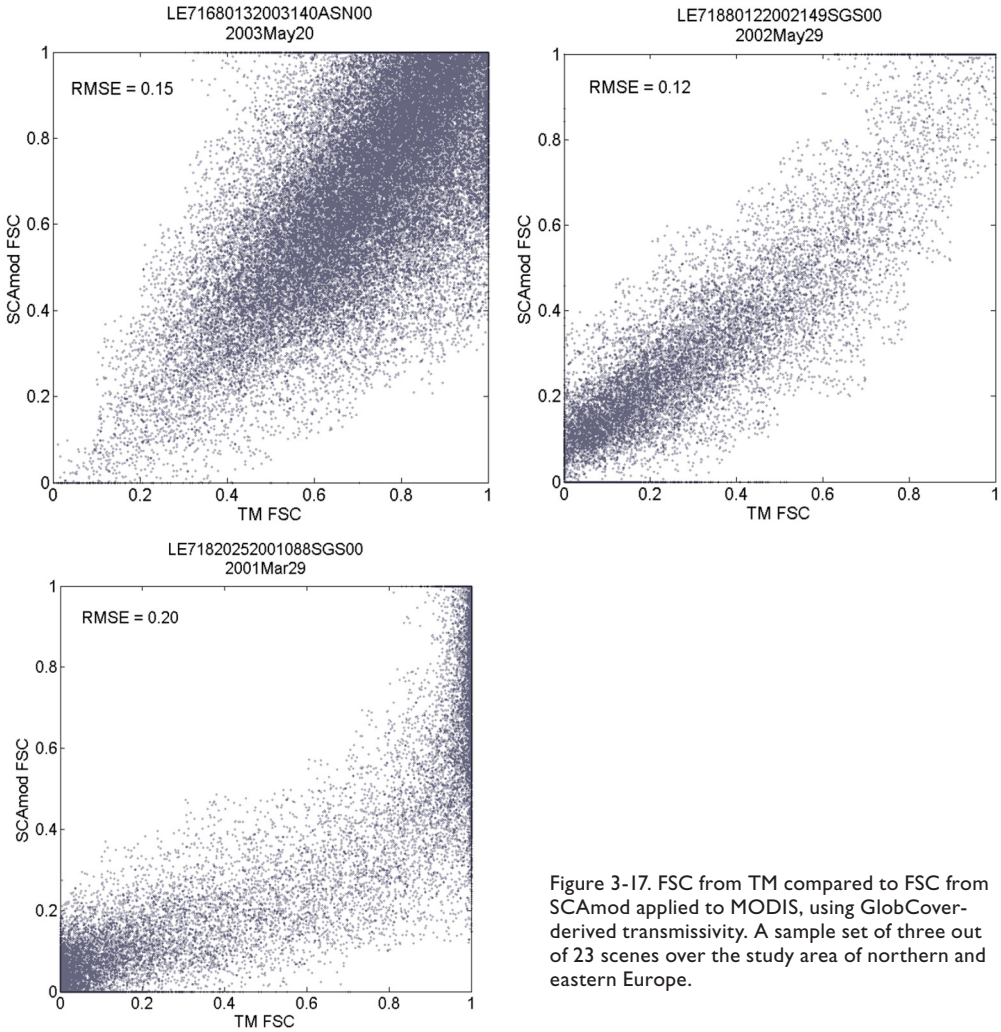

Figure 3-17. FSC from TM compared to FSC from SCAmod applied to MODIS, using GlobCover-derived transmissivity. A sample set of three out of 23 scenes over the study area of northern and eastern Europe.

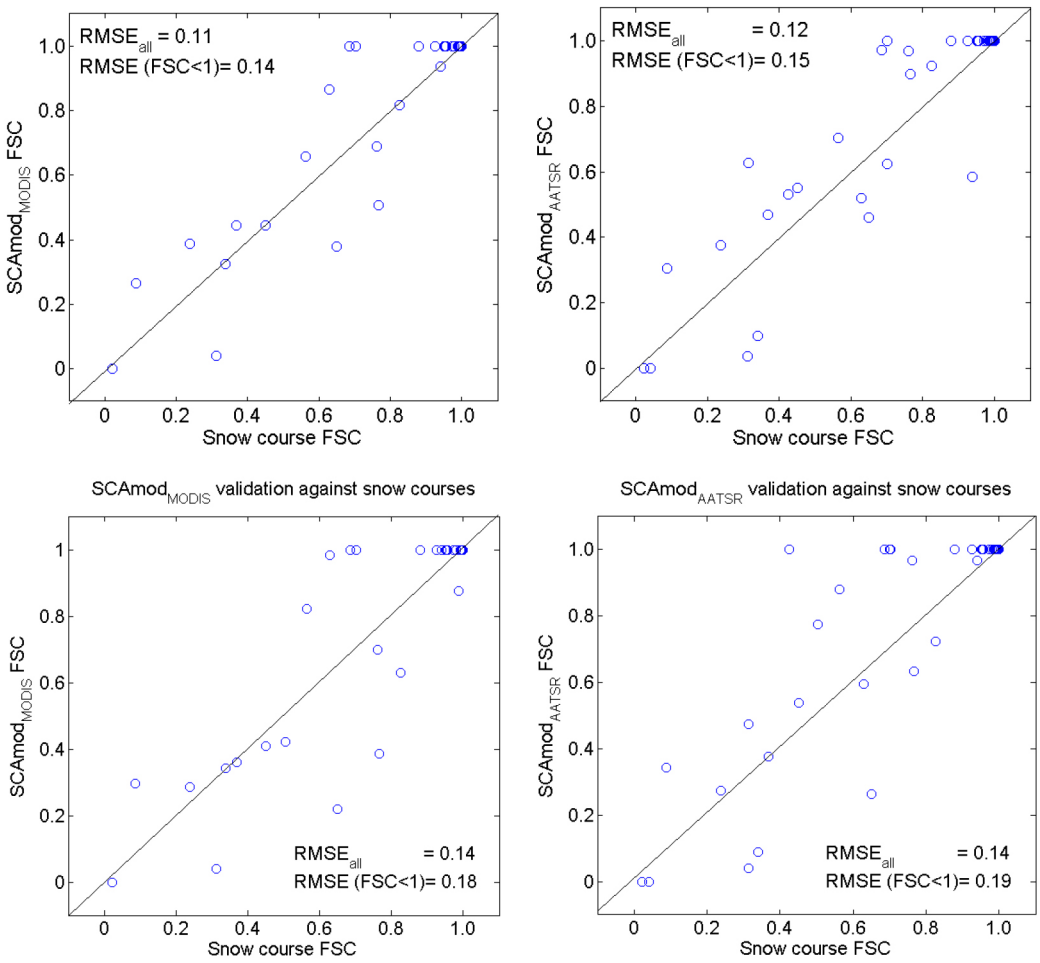

Figure 3-18. Validation against Finnish snow course observations for SCAmod applied to MODIS and AATSR when MODIS-derived tranmissivity is employed (upper pane), and the corresponding results when GlobCover-derived transmissivity is used (lower pane).

3.5 Future prospects

Future work will focus on improvements to SCAmod. This work has already started with an attempt to still better account for dense forest areas. Although the general performance of SCAmod employing GlobCover-derived transmissivity ($trans_{GC}$) was shown to be good, some underestimations typically occur for very dense forests. This can be seen e.g. in Fig. 3-19 presenting the GlobSnow monthly average FSC-map from March 2003: some evident underestimations are exhibited for Russian boreal forests while the surrounding areas have 100% snow cover. Clearly, these underestimations follow the spatial patterns of dense forests. It was found that the proposed approach for continental transmissivity generation cannot fully catch the densest forest, i.e. too high transmissivities are often obtained compared to original MODIS-derived values. Comparison between distributions of $trans_{MODIS}$ and $trans_{GC}$ for one of the teaching areas, Russia (west from the Ural mountains, area 2.3 million km^2), is presented in Fig. 3-21 (left) . This area represents very dense conifer forest canopies in some parts. It can be seen from the transmissivity distribution

that the lowest transmissivities are missed in $trans_{GC}$. High transmissivities are also not properly caught. This evidently has implications for fractional snow cover estimates. For dense forests this is seen as underestimations of FSC, and for open areas as overestimations. Although these issues will be investigated more in future work, some studies have already been made and the resulting suggestions for improvements are discussed in the following.

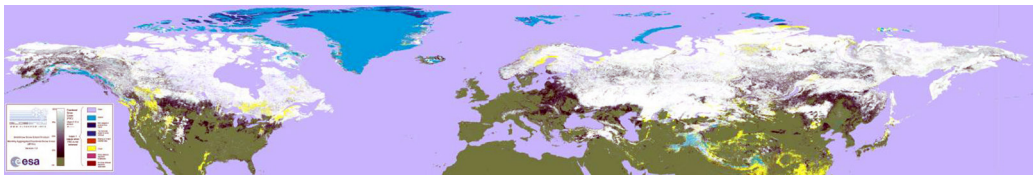

Figure 3-19. A monthly-aggregated map of Fractional snow cover, March 2003. GlobSnow Snow Extent v1.2, www.globsnow.info. White color indicates full snow cover, lower snow fractions are presented in different shades of grey while green color indicates snow-free ground.

The analysis of the spatial patterns of discrepancies between $trans_{GC}$ and $trans_{MODIS}$ revealed that most problems occur with four particular boreal forest classes. In continental-scale GlobCover-data, these classes appear to represent both very dense and moderately dense forests, implying that a wide distribution of transmissivities is assigned to each of these classes in the teaching areas. As a result, the obtained average transmissivity does not properly represent either of the forest types. Therefore it was concluded that the GlobCover-based approach would benefit from external data accounting for the forest density.

Compared to other land covers, *albedo* from boreal forest is low throughout the year, but the contrast in winter is even greater. Although there is an increase in albedo over snow-covered (snow on or below the canopy) boreal forests, these albedos clearly differ from those from non-forested areas (Betts and Ball, 1997; Barlage et al., 2005; Moody et al., 2007). Hence it was decided to test the feasibility of wintertime global albedo-data in discriminating between moderate and dense forests. According to Manninen and Stenberg (2009), red-band white-sky albedo from snow-covered (snow below the canopy) boreal forest is dominated by the bidirectional transmissivity to and from the forest floor, whereas NIR-albedo is predominantly affected by canopy scattering (direct or after interaction with the forest floor). Therefore in this study, visible albedo was considered to have the best correlation with transmissivity and therefore should be a good candidate in identification of the most dense forests. For Eurasia, the ESA GlobAlbedo (Muller et al., 2012) white-sky visible albedo from two 8-day composites was used in identifying the densest forests. This time-frame was selected to best avoid measurement of the albedo from snow-covered canopy, as this would hamper the results (snow-on-canopy raises the albedo particularly in mid-winter but more rarely in March, e.g. Kuusinen et al., 2012). White-sky albedo was chosen, as it is independent of the angular effects. The albedo map in 0.05°×0.05° grid was resampled into 0.01°×0.01° grid in order to make it compatible with the GlobSnow processing grid.

A high linear correlation between the albedo – with snow cover on terrain prevailing – and MODIS-derived transmissivity was found, particularly around very low transmissivity and albedo. Hence it was concluded that the specified four GlobCover forest classes can be divided into two categories, moderate and dense, according to their albedo. The threshold for judging between these two was set to 0.15, based on results by Betts and Ball (1997) as well as on empirical tests with $trans_{MODIS}$ and GlobAlbedo data. The corrections to the continental transmissivity map were carried out for pixels dominated by one of the four classes or mixtures of them, and at the same time showing albedo less than the threshold, i.e. representing dense forest. The linear fitting parameters gained from the analysis described above were applied to decrease the original transmissivity relative to the albedo. It should be noted that this technique is valid only in the presence

of full snow cover, correspondingly to transmissivity calculations as presented in Metsämäki et al., (2005, 2012). Therefore, snow information from the global GlobSnow Snow Water Equivalent (SWE) product (Takala et al., 2011) from March 2005 was used to identify the snow-covered areas before launching the procedure.

Some other changes are obvious when comparing the obtained new transmissivity with the earlier version (see Figs. 3-20 and 3-15). These are mainly because of the employment of new teaching areas (one in eastern Eurasia covering vast areas of needle-leaved deciduous forests and another in North America covering boreal forests, tundra and grassland) which provided updates to the original transmissivity statistics. These matters are not discussed here, as the intention is only to demonstrate the use of albedo in transmissivity calculations.

The new more representative two-way transmissivity map (hereafter referred to as $trans_{GC+a}$) for Eurasia is presented in Fig. 3-20. A comparison between distributions of $trans_{MODIS}$ and $trans_{GC+a}$, again for Russia, is presented in Fig. 3-21 (right). The low transmissivities i.e. dense forests are now significantly better caught. Employing the new transmissivity map, SCAmod is expected to provide a clearly better performance for dense forests. The preliminary results for a dense forest area over the Finnish-Russian border are presented in Table 3-3, where FSC retrievals from TM and SCAmod with all three transmissivities are assessed in terms of RMSE, average FSC and *Recall*. The scene area is discerned to be fully snow-covered according to weather station observations, GlobSnow SWE and general climatology. Hence, any deviation from FSC=1 is considered

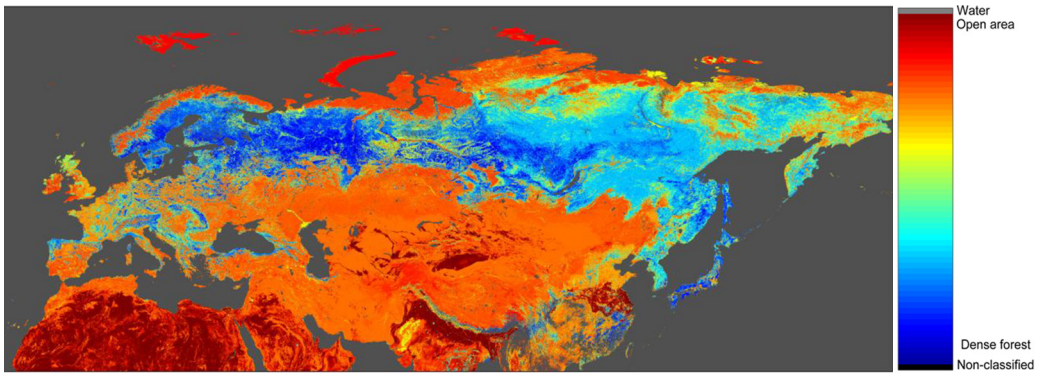

Figure 3-20. Two-way transmissivity (t^2, range 0-1) for Eurasia, using GlobCover-data and GlobAlbedo-data as an additional data source to teaching area-based MODIS-derived transmissivity.

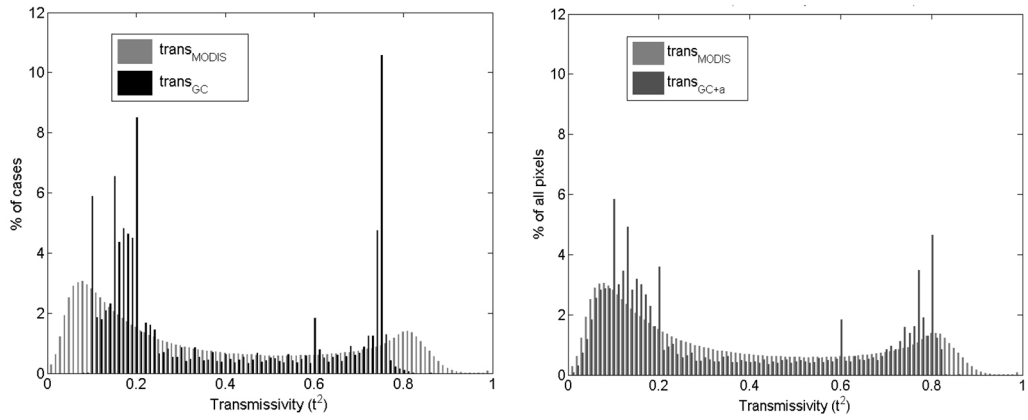

Figure 3-21. The MODIS-derived transmissivities and the GlobCover-derived transmissivities for western Russia when *Left*: GlobCover-data is employed, *Right*: GlobCover-data and GlobAlbedo data are employed.

an underestimation. This is well described by RMSE, using FSC=1 as $FSC_{reference}$ (see Eq. 2-1). The average scene FSC approaching 1 is also a measure of good performance. Recall is provided using *a priori* known FSC=1 as 'snow', considering any deviation from that as 'not snow'. This assessment is an addition to the analysis presented in Table 7 of **[P4]**, to demonstrate the potential of using albedo in transmissivity determination. The resulting FSC-maps for visual interpretations are presented in Appendix II.

From the above results, it is clear that the albedo-based approach is feasible for corrections of transmissivity values derived from GlobCover data. It should be noted, however, that the need of correction depends on how well the applied land-cover data discriminates the different forests in the first place (in terms of transmissivity or crown coverage at least). While relying on GlobCover-data or equivalent, the work for transmissivity improvement will continue, as well as the development work related to SCAmod itself. There are on-going investigations of the relationship between transmissivity and crown cover/tree height; the impact of snow-on-canopy on the observed reflectance and its implication for FSC-retrievals using SCAmod is also currently being studied. It is assumed that SCAmod itself is feasible in describing the reflectance from snow-covered forest (and also from non-forested areas). However, the work towards verifying the model with reflectance observations at different scales – at ground, at tower, airborne, satellite-borne – will continue. These efforts include also investigations on SCAmod performance in mountain regions; in ESA DUE-project GlobSnow-2 (2012-2014), northern hemisphere FSC maps are provided for mountain and non-mountain areas (after topographic correction of top-of-atmosphere reflectances). These FSC retrievals are currently under validation. The preliminary results indicate a good performance of SCAmod for both terrain types.

Table 3-3. The effect of different transmissivities on SCAmod FSC over fully snow covered dense boreal forest area.

Scene	Recall (%)		RMSE [0-1]		Average FSC [0-1]		transmissivity t^2	Number of pixels
	ETM+	SCAmod	ETM+	SCAmod	ETM+	SCAmod		
#24 186/017 15 March 2003	5.43	60.66 t_{MODIS} 71.50 t_{GC} 82.80 t_{GC+a}	0.32	0.28 t_{MODIS} 0.27 t_{GC} 0.21 t_{GC+a}	0.79	0.86 t_{MODIS} 0.88 t_{GC} 0.93 t_{GC+a}	0.19 t_{MODIS} 0.14 t_{GC} 0.11 t_{GC+a}	11190
#25 174/016 09 April 2002	24.10	87.56 t_{MODIS} 59.20 t_{GC} 71.08 t_{GC+a}	0.26	0.12 t_{MODIS} 0.28 t_{GC} 0.20 t_{GC+a}	0.84	0.97 t_{MODIS} 0.84 t_{GC} 0.91 t_{GC+a}	0.09 t_{MODIS} 0.12 t_{GC} 0.10 t_{GC+a}	22639

4 Conclusions

In this work, the basic principles and development work of a method for mapping of fractional snow cover (FSC) using optical remote sensing data were described. From the very beginning, the aim was to develop a feasible method for snow mapping, particularly in boreal forest areas where the majority of other existing methods usually fail due to the masking effects of forest canopies. The development work started with linear interpolation techniques in which the forest canopy effect was considered in locally determined reference values representing full snow cover and snow-free conditions. Although good results were obtained for Finland, there was a need to develop a more physically-based method that could then be used in further investigations and improvements e.g. using field spectroscopy. The basic idea of accounting for canopy obscurance by employing the canopy transmissivity via a radiative transfer-based reflectance model was shown to be very feasible in fractional snow mapping. The relatively simple formulation of the model enables its use in continental-scale snow mapping, as it does not consider detailed forest characteristics but only the apparent (from a satellite sensor point of view) effect of canopy obscurance on the observed reflectance. This means that the methodology, named *SCAmod,* is easily adaptable to extensive regions and also to new satellite sensors as long as these are operating at optical wavelengths.

Through validation against *in situ* measurements, the developed methodology was demonstrated to provide Fractional snow cover with a good accuracy even for boreal forest areas. The gained root-mean-squared-error (RMSE) was less than 0.15 in the FSC range 0-1 i.e. less than 15%. Since *in situ* measurements on fractional snow cover were available only from Finnish snow transects, validation work for areas outside Finland was based on comparisons against reference FSC derived from high-resolution Earth-observation data. Although this kind of approach has its drawbacks since the reference data does not necessarily represent the 'truth' and can be biased, a good agreement between high-resolution Landsat/TM-based FSC and SCAmod-based FSC was obtained. In fact, the experiment with reflectance data acquired at *a priori* known full snow cover conditions proved that the SCAmod method performs better than the reference data at least in dense forest areas, so that the obtained discrepancies may favour SCAmod over the reference data source. From the analyses with data acquired at full snow cover conditions, it was also evident that SCAmod performance does not significantly deteriorate according to forest density, which is a benefit when particularly undercanopy snow is targeted, e.g. for hydrological applications. These demonstrations suggest that the developed method has high potential for large scale fractional snow mapping particularly in the boreal forest zone, but also outside forested areas.

References

Anttila, S., Metsämäki, S., & Derksen, C. (2006). A comparison of Finnish SCAmod Snow Maps and MODIS Snow Maps in Boreal Forests in Finland and in Manitoba, Canada. In: *Proceedings of IEEE International Geoscience and Remote Sensing Symposium (IGARSS 2006)*, July 31–August 4 2006, Denver, Colorado, USA. pp. 2176–2179.

Barlage, M., Zeng, X., Wei, H. & Mitchell, K. (2005). A global 0.05º maximum albedo dataset of snow-covered land based on MODIS observations. *Geophysical Research Letters,* 32: L17405.

Betts, A. K. & Ball, J. H. (1997). Albedo over the boreal forest. *Journal of Geophysical Research*, 102(D24): 28901–28909.

Bicheron, P., Defourny, P., Brockmann, C., Schouten, L., Vancutsem, C., Huc, M., Bontemps, S., Leroy, M., Achard, F., Herold, M., Ranera, F. & Arino, O. (2008). *GLOBCOVER Products Description and Validation Report*. Medias France, Toulouse, France. Available at: http://due.esrin.esa.int/globcover/LandCover_V2.2/GLOBCOVER_Products_Description_Validation_Report_I2.1.pdf

Choi, G., Robinson, D. A. & Kang, S. (2010). Changing Northern Hemisphere Snow Seasons. *Journal of Climate*, 23: 5305–5310.

Cihlar, J., Manak, D. & Voisin, N. (1994). AVHRR bidirectional reflectance effects and compositioning. *Remote Sensing of Environment*, 48: 77–88.

Dozier, J., Schneider, S. R. & McGinnis Jr., D. F. (1981). Effect of grain size and snow water equivalence on visible and near-infrared satellite observation of snow. *Water Resources Research*, 17: 1213–1221.

Dozier, J. (1989). Spectral signature of alpine snow cover from the Landsat Thematic Mapper. *Remote Sensing of Environment*, 28: 9–22.

Dumont, M., Brissaud, O., Picard, G., Schmitt, B., Gallet, J.-C. & Arnaud, Y. (2010). High-accuracy measurements of snow Bidirectional Reflectance Distribution Function at visible and NIR wavelengths – comparison with modelling results. *Atmospheric Chemistry and Physics*, 10: 2507-2520.

Fily, M., Bourdelles, B., Dedieu, J. P. & Sergent, C. (1997). Comparison of in situ and Landsat Thematic Mapper derived snow grain characteristics in the Alps. *Remote Sensing of Environment*, 59: 452–460.

Frei, A., Tedesco, M., Lee, S., Foster, J., Hall, D. K., Kelly, R. & Robinson, D. A. (2012). A review of global satellite-derived snow products. *Advances in Space Research*, 50: 1007–1029.

Golding, D. L. & Swansson, R. H. (1986). Snow distribution patterns in clearings and adjacent forest. *Water Resources Research*, 22: 1931–1940.

Gong, G., Cohen, J., Entekhabi, D. & Ge, Y. (2007). Hemispheric-scale climate response to Northern Eurasia land surface characteristics and snow anomalies. *Global and Planetary Change*, 56: 359–370.

Groisman, P. Y., Karl, T. R. & Knight, R. W. (1994). Changes of snow cover, temperatures and radiative heat balance over the Northern Hemisphere. *Journal of Climate,* 7: 1633–1656.

Hall, D. K., Foster, J. L., Chang, A. T. C., Benson, C. S. & Chien, J. Y. L. (1998). Determination of snow-covered area in different land covers in central Alaska from aircraft data-April 1995. *Annals of Glaciology*, 26: 149–l55.

Hall, D. K., Riggs, G. A. & Salomonson, V. V. (1995). Development of methods for mapping global snow cover using moderate resolution imaging spectroradiometer data. *Remote Sensing of Environment*, 54: 127–140.

Hall, D. K., Riggs, G.A. & Salomonson, V. V. (2006a). MODIS Snow and Sea Ice Products. In: Qu, J. J., Gao, W., Kafatos, M., Murphy, R. E. & Salomonson, V. V. (eds.), *Earth Science Satellite Remote Sensing -Volume I*: Science and Instruments. Springer, New York.

Hall, D. K., Riggs, G. A. & Salomonson, V. V. (2006b). *MODIS/Terra Snow Cover 5-min L2 Swath 500m V005*, [2003–2010]. Digital media, updated daily. Boulder, Colorado USA: National Snow and Ice Data Center. Available at: http://nsidc.org/data/docs/daac/modis_v5/mod10_l2_modis_terra_snow_cover_5min_swath.gd.html

Hall, D. K. & Riggs, G. A. (2007). Accuracy assessment of the MODIS snow products. *Hydrological Processes*, 21: 1534–1547.

Jin, Z. & Simpson, J. J. (1999). Bidirectional anisotropic reflectance of snow and sea ice in AVHRR channel 1 and 2 spectral regions — Part I: theoretical analysis. *IEEE Transactions on Geoscience and Remote Sensing,* 37: 543–554.

Kitaev, L., Kislov, A., Krenke, A., Razuvaev, V., Martuganov, R. & Konstantinov, I. (2002). The snow characteristics of northern Eurasia and their relationship to climatic parameters. *Boreal Environment Research,* 7: 437–445.

Kite, G. & Pietroniro, A. (1996). Remote sensing applications in hydrological modeling. *Hydrological Sciences Journal*, 41: 563–591.

Klein, A. G., Hall, D. K. & Riggs, G. A. (1998). Improving snow-cover mapping in forests through the use of a canopy reflectance model. *Hydrological Processes*, 12: 1723–1744.

Koskinen, J. T., Pulliainen, J. T. & Hallikainen, M. T. (1997). The use of ERS-1 SAR data in snow melt monitoring. *IEEE Transactions on Geoscience and Remote Sensing*, 35: 601–610.

Kuusinen, N. J., Kolari, P., Levula, J., Porcar-Castell, A., Stenberg, P. & Berninger, F. (2012). Seasonal variation in boreal pine forest albedo and effects of canopy snow on forest reflectance. *Agricultural and Forest Meteorology*, 164: 53–60.

Kuusisto, E. (1984). *Snow accumulation and snowmelt in Finland*. National Board of Waters, Helsinki.

Liu, J., Woodcock, C., Melloh, R., Davis, R., McKenzie, C. & Painter, T. (2008). Modeling the view angle dependence of gap fractions in forest canopies: Implications for mapping fractional snow cover using optical remote sensing. *Journal of Hydrometeorology*, 9: 1005–1019.

Luojus, K., Pulliainen, J., Rott, H., Nagler, T., Solberg, R., Wiesmann, A., Derksen, C., Metsämäki, S., Malnes, E. & Bojkov, B. (2010). ESA DUE GlobSnow — Global snow database for climate research. In: *Proceedings of ESA Living Planet Symposium*, June 28– July 2, Bergen, Norway.

Manninen, T. & Stenberg, P. (2009). Simulation of the effect of snow covered forest floor on the total forest albedo. *Agricultural and Forest Meteorology*, 149: 303–319.

Matikainen, L., Kuittinen, R. & Vepsäläinen, J. (2002). Estimating drainage area-based snow cover percentages from NOAA/AVHRR images. *International Journal of Remote Sensing*, 23: 2971–2988.

METLA (2009). Finnish Statistical Yearbook of Forestry 2009. Finnish Forest Research Institute, Helsinki.

Metsämäki, S., Vepsäläinen, J., Pulliainen, J. & Sucksdorff, Y. (2002). Improved linear interpolation method for the estimation of snow-covered area from optical data. *Remote Sensing of Environment*, 82: 64–78.

Metsämäki, S., Anttila, S., Huttunen, M. & Vepsäläinen, J. (2005). A feasible method for fractional snow cover mapping in boreal zone based on a reflectance model. *Remote Sensing of Environment*, 95: 77-95.

Metsämäki, S., Mattila, O.-P., Pulliainen, J., Niemi, K., Luojus, K. & Böttcher, K. (2012). An optical reflectance model-based method for fractional snow cover mapping applicable to continental scale. *Remote Sensing of Environment*, 123: 508–521.

Moody, E. G., King, M. D., Schaaf, C. B. & Hall, D. K. (2007). Northern Hemisphere five-year average (2000–2004) spectral albedos of surfaces in the presence of snow: Statistics computed from Terra MODIS land products. *Remote Sensing of Environment*, 111: 337–345.

Muller, J.-P., Lopez, G., Watson, G., Shane, N., Kennedy, T., Yuen, P., Lewis, P., Fischer, J., Guanter, L., Domench, C., Presusker, R., North, P., Heckel, A., Danne, O., Krämer, U., Zühlke, M., Brockmann, C. & Pinnock, S. (2012). The ESA GlobAlbedo Project for mapping the Earth's land surface albedo for 15 Years from European Sensors. In: *Proceedings of IEEE Geoscience and Remote Sensing Symposium (IGARSS 2012)*, 22–27 July 2012, Munich, Germany.

Nolin, A.W. & Dozier, J. (2000). A hyperspectral method for remotely sensing the grain size of snow. *Remote Sensing of Environment*, 74: 207–216.

Nolin, A. (2004). Towards retrieval of forest cover density over snow from the Multiangle Imaging SpectroRadiometer (MISR). *Hydrological Processes*, 18: 3623–3636.

Painter, T. H., Dozier, J., Roberts, D. A., Davis, R. E. & Green, R. O. (2003). Retrieval of subpixel snow-covered area and grain size from imaging spectrometer data. *Remote Sensing of Environment*, 85: 64–77.

Painter, T. H. & Dozier, J. (2004). Measurements of the hemispherical–directional reflectance of snow at fine spectral and angular resolution. *Journal of Geophysical Research-Atmospheres*, 109: D18115.

Painter, T. H., Rittger, K., McKenzie, C., Slaughter, P., Davis, R. E. & Dozier, J. (2009). Retrieval of subpixel snow covered area, grain size, and albedo from MODIS. *Remote Sensing of Environment*, 113: 868–879.

Peltoniemi, J., Kaasalainen, S., Näränen, J., Matikainen, L. & Piironen, J. (2005). Measurement of directional and spectral signatures of light reflectance by snow. *IEEE Transactions on Geoscience and Remote Sensing*, 43: 2294–2304.

Pulliainen, J., Heiska, K., Hyyppä, J. & Hallikainen, M. (1994). Backscattering properties of boreal forests at the C- and X-band. *IEEE Transactions on Geoscience and Remote Sensing*, 32: 1041–1050.

Rahman, H. & Dedieu, G. (1994). SMAC: a simplified method for the atmospheric correction of satellite measurements in the solar spectrum. *International Journal of Remote Sensing*, 15: 123–143.

Riggs, G. A., Hall, D. K. & Salomonson, V. V. (1994). A snow index for the Landsat Thematic Mapper and Moderate Resolution Imaging Spectroradiometer. In: *Proceedings of the International Geoscience and Remote Sensing Symposium (IGARSS 1994)*, 8–12 August 1994, Pasadena, California, USA. pp. 1942–1944.

Riggs, G. A., Hall, D. K. & Salomonson, V. V. (2006). *MODIS Snow Products User Guide to Collection 5*. Available at: http://nsidc.org/data/docs/daac/modis_v5/dorothy_snow_doc.pdf

Rittger, K., Painter, T. H. & Dozier, J. (2012). Assessment of methods for mapping snow cover from MODIS. *Advances in Water Resources*, 51: 367–380.

Robinson, D. A. & Kukla, G. (1985). Maximum surface albedo of seasonally snow-covered lands in the Northern Hemisphere. *Journal of Climatology and Applied Meteorology*, 23: 402–411.

Robinson, D. A. & Frei, A. (2000). Seasonal Variability of Northern Hemisphere Snow Extent using Visible Satellite Data. *Professional Geographer*, 52: 307–314.

Roesch, A. & Roeckner, E. (2006). Assessment of snow cover and surface albedo in the ECHAM5 general circulation model. *Journal of Climate*, 19: 3828–3843.

Salomonson, V. V. & Appel, I. (2004). Estimating fractional snow cover from MODIS using the normalized difference snow index. *Remote Sensing of Environment*, 89: 351–360.

Salomonson, V. V. & Appel, I. (2006). Development of the Aqua MODIS NDSI fractional snow cover algorithm and validation results. *IEEE Transactions on Geoscience and Remote Sensing*, 44: 1747–1756.

Schaepman-Strub, G., Schaepman, M. E., Painter, T. H., Dangel, S. & Martonchik, J. V. (2006). Reflectance quantities in optical remote sensing — Definitions and case studies. *Remote Sensing of Environment*, 103: 27–42.

Schlerf, M. & Atzberger, C. (2006). Inversion of a forest reflectance model to estimate structural canopy variables from hyperspectral remote sensing data. *Remote Sensing of Environment*, 100: 281–294.

Schmugge, T. J., Kustas, W. P., Ritchie, J., Jackson, T. & Rango, A. (2002). Remote sensing in hydrology. *Advances in Water Resources*, 25: 1367–1385.

Sellers, P. J. (1989). Vegetation canopy spectral reflectance and biophysical processes. In: Asrar, G. (ed.), *Theory and Applications of Optical Remote Sensing*. Wiley, New York. pp. 297-335.

Steffen, K. (1987). Bidirectional reflectance of snow at 500 - 600 nm. In: Goodison, B. E., Barry, R. G. & Dozier, J. (eds.), *Large scale effects of seasonal snow cover*. IAHS, Wallingford, UK. pp. 415–425.

Stow, D. A., Hope, A, McGuire, D., Verbyla, D., Gamon, J., Huemmrich, F., Houston, S., Racine, C., Sturm, M., Tape K., Hinztman, L., Yoshikawa., K., Tweedie, C., Noyle, B., Silapaswan, C., Douglas, D., Griffith, B., Jia, G., Epstein, H., Walker, D., Daeschner, S., Petersen, A., Zhou, L. & Myneni, R. (2004). Remote sensing of vegetation and land-cover change in Arctic tundra ecosystems. *Remote Sensing of Environment*, 89: 281–308.

Stöckli, R. & Vidale, P. L. (2004). European plant phenology and climate as seen in a 20 year AVHRR land-surface parameter dataset. *International Journal of Remote Sensing*, 25, 3303–3330.

Takala, M., Luojus, K., Pulliainen, J., Derksen, C., Lemmetyinen, J., Kärnä, J. -P., Koskinen, J. & Bojkov, B. (2011). Estimating northern hemisphere snow water equivalent for climate research through assimilation of space-borne radiometer data and groundbased measurements. *Remote Sensing of Environment*, 115: 3517–3529.

Taylor, J. R. (1982). *An introduction to error analysis: The study of uncertainties in physical measurements*. University Science Books, Mill Valley, California.

Vikhamar, D. & Solberg, R. (2003). Subpixel mapping of snow cover in forests by optical remote sensing. *Remote Sensing of Environment*, 84: 69–82.

Vikhamar, D., Solberg, R. & Seidel, K. (2004) . Reflectance modelling of snow-covered forests in hilly terrain. *Remote Sensing & Photogrammetrical Engineering*, 70: 1069–1079.

Viterbo, P. & Betts, A. K. (1999). Impact on ECMWF forecasts of changes to the albedo of the boreal forests in the presence of snow. *Journal of Geophysical Research*, 104(D22): 27803–27810.

Warren, S. G. (1982). Optical properties of snow. *Reviews of Geophysics and Space Physics*, 20: 67–89.

Wiscombe,W. J. & Warren, S. G. (1980). A model for the spectral albedo of snow. I: pure snow. *Journal of the Atmospheric Sciences*, 37: 2712–2733.

Xin, Q. C., Woodcock, C. E., Liu, J. C., Tan, B., Melloh, R. A. & Davis, R. E. (2012). View angle effects on MODIS snow mapping in forests. *Remote Sensing of Environment,* 118: 50–59.

Appendix I.

According to the radiation transfer theory, inside absorptive and scattering media, radiance attenuates in distance s as follows:

$$\frac{dL}{ds} = -\kappa_e L \Leftrightarrow \int_{L_0}^{L} \frac{dL}{L} = \int_0^s -\kappa_e ds' \Leftrightarrow \ln(L) - \ln(L_0) = -\kappa_e \cdot s \Leftrightarrow \ln\left(\frac{L}{L_0}\right) = -\kappa_e \cdot s$$

$$\Leftrightarrow \frac{L}{L_0} = e^{-\kappa_e \cdot s} \Leftrightarrow L = L_0 \cdot e^{-\kappa_e s}$$

where L_o and L are the incoming and attenuated radiances, respectively. κ_e is the extinction coefficient of the media: $\kappa_e = \kappa_a + \kappa_s$, where κ_a *and* κ_s are the absorption and scattering coefficients, respectively.

The reflected radiance into the backscattering direction (assuming that the illumination and viewing directions are the same) is

$$L_{back}(s) = \int_0^s L_0 e^{-\kappa_e s'} \rho_v(s') \cdot e^{-\kappa_e s'} ds' = \int_0^s L_0 e^{-2\kappa_e s'} \rho_v(s')$$

$$\Rightarrow \frac{L_{back}(s')}{L_0} = R_{back} = \int_0^s e^{-2\kappa_e s'} \rho_v(s') ds',$$

where R_{back} is the reflectance and $\rho_v(s')$ is the (bidirectional) scattering/reflection coefficient. If $\rho_v(s')$ is constant within the media (forest canopy), we get

$$R_{back} = \rho_v \int_0^s e^{-2\kappa_e s'} ds' = \rho_v \left[\frac{1}{-2\kappa_e} e^{-2\kappa_e \cdot s} - \frac{1}{-2\kappa_e} e^{-2\kappa_e \cdot 0} \right] = \rho_v \frac{1}{-2\kappa_e} \left[e^{-2\kappa_e s} - 1 \right] = \frac{\rho_v}{2\kappa_e} \left[1 - e^{-2\kappa_e s} \right]$$

By definition, transmissivity $t = e^{-\int_0^s \kappa_e(s')ds'} = e^{-\kappa_e s}$, given that κ_e is constant. Hence, we get

$$R_{back} = \frac{\rho_v}{2\kappa_e} \left[1 - t^2 \right] = R_{forest} \left[1 - t^2 \right].$$

The latter is true, since if $s \to \infty$, then $\frac{\rho_v}{2\kappa_e} \to R_{back}$ with every value of κ_e.

Accordingly, $R_{back} \to R_{forest}$, where R_{forest} is the reflectance of opaque forest canopy.

Appendix II.

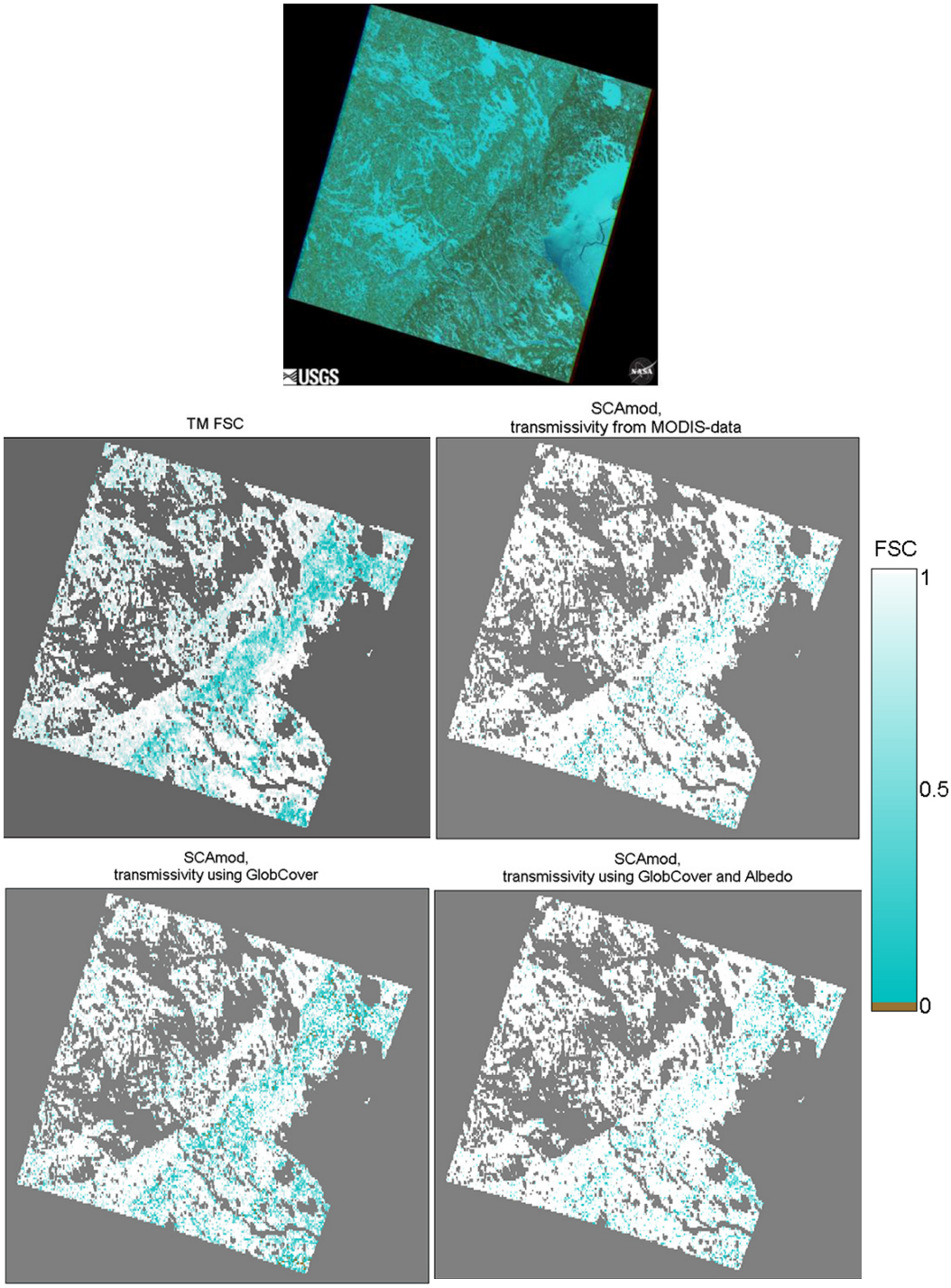

TM-derived FSC and SCAmod-derived FSC (SCAmod applied to MODIS-data) for a fully snow-covered area also including very dense forest (dark area visble in the top image). *TopLeft:* TM FSC, showing underestimations over forests, *TopRight:* SCAmod FSC with MODIS-derived transmissivity, *BottomLeft:* SCAmod FSC with GlobCover-derived transmissivity and *BottomRight:* SCAmod FSC using transmissivity derived from GlobCover+GlobAlbedo.

ISBN 978-952-93-2556-6 (pbk.)
ISBN 978-952-93-2557-3 (PDF)

Edita Prima Ltd
Helsinki 2013, Finland